Magnetohydrodynamic Effect on Two-Phase Flow in the porous medium through a Rectangular Curved Duct

Md. Khalilur Rahman (khalil33bcs@gmail.com)
Bangladesh University of Engineering & Technology
Salma Parvin
Bangladesh University of Engineering & Technology
Md. Abdul Hakim Khan
Bangladesh University of Engineering & Technology

Research Article

Keywords: Rectangular Curved Duct, Dean number, Magnetohydrodynamic, Two-phase flow, Porous Medium

Posted Date: December 21st, 2022

DOI: https://doi.org/10.21203/rs.3.rs-2384884/v1

Additional Declarations: No competing interests reported.

Magnetohydrodynamic Effect on Two-Phase Flow in the porous medium through a Rectangular Curved Duct

Md. Khalilur Rahman[1,2*], Salma Parvin[2, *], Md. Abdul Hakim Khan[2]

[1]Department of Mathematics, Bangladesh Civil Service, Ministry of Education, Dhaka-1000, Bangladesh

[2]Department of Mathematics, Bangladesh University of Engineering & Technology, Dhaka-1000, Bangladesh

*corresponding author: khalil33bcs@gmail.com

Keywords: *Rectangular Curved Duct; Dean number; Magnetohydrodynamic; Two-phase flow; Porous Medium.*

Abstract

For the best structure and reliable maintenance, two- or multiphase flow is becoming more and more essential in engineering systems. However, a variety of different of biological organisms and natural phenomena that exhibit two-phase situations can be explored to improve our knowledge of this. This is so because current industrial technology does not place these limitations. This research aims to investigate the effect of an external magnetic field on unsteady laminar incompressible two-phase flow in a porous medium via a rectangular curved duct. The relevant governing equations are represented by the Navier-Stokes equations and by the Level set equation with boundary conditions. Fluid flow through curved rectangular ducts behaves differently from fluid flow through straight ducts due to the centrifugal action generated by duct curvature. Within curved ducts, centrifugal force is generated secondary flow vortices and spiraling fluid motion. This analysis graphically depicts the fluid phase distribution, the Dean vortex, velocity contours, and fluid volume fractions. Furthermore, displayed are the effects of the aspect ratio, porosity, Dean number, radius of curvature, and Hartmann number. Additionally, a comparison of two-phase flow between various fluids is presented.

Introduction

Fluid mechanics is fundamentally interested in the flow of curved ducts or pipes, as well as in practical problems in many applications. Products like this channel or duct are produced in nations that produce oil. It is particularly significant in engineering, including biological transport phenomena, heat exchangers, aviation intake diffusers, and turbomachinery blade tunnels. The

existence of a secondary rotational motion caused by curvature that is perpendicular to the stream wise flow direction was first analytically demonstrated Eustice [1, 2] and later theoretically investigated by Dean [3, 4]. Dean vortex-based secondary flow is caused by a difference in the stream wise velocity of the fluid in the channel center and near the wall. Although there have been many relevant and important studies (Thangnam and Hur [5, 6], Khuri [7], Nadeem and Shahzadi [8, Mondal et al. [8, 9], and Yamamoto et al. [10], there have not been enough focus on the creation and development of secondary flow curved duct flow (laminar flow, Stokes flow, peristaltic flow, non-isothermal flow, Dean flow). In particular, numerous experimental research on flow investigation in a constant area curved duct have been conducted (Dong and Ebadian [11], Ligrani and Hedland [12], Avramenko et al. [13], Biswas et al. [14]. Flow on non-aligned straight rotating pipes and curved pipes has been critically examined by Hye and Khan [15, 16] as well.

In many industrial applications, non-mixing multi-component fluid flows are popular. A few of these examples are the transportation of crude oil mixed with water in the oil and gas industry, the chemical fluid flow within reactors in pharmaceutical production processes [17], and the flow of lubricant and refrigerant mixtures in refrigeration systems [18, 19]. The study of two phase flow therefore represents a factors that help for researchers. The discipline has seen the completion of numerous significant investigations, many of which are still ongoing (Okechi and Asghar [20], Garg et al. [21], and Jason [22]). Various experimentally investigated on multiphase flow have been carried out (Xu et al. [23], Crandall et al. [24], Kishor et al. [25], and Al-Jibory et al. [26]).

The study of the dynamics of electrically conducting fluids is known as magnetohydrodynamics (MHD), which is a combination of the Navier-Stokes equations for fluid dynamics and Maxwell's equations for electromagnetism. The main principle of the MHD is that magnetic fields can generate currents in moving conductive fluids, which in turn apply forces on the fluid and affect the magnetic field. MHD flow has received a significant amount of attention from researchers because of its potential applications. Haque and Alam [27], Chen et al. [28], and Vaidya et al. [29] examined the MHD influence on several fluid types. The

stability of magnetohydrodynamics for various types of channel flow was computationally investigated by Md. S. Alam et al. [30–32] and M.K. Rahman et al. [33].

Engineers and scientists are fascinated by the flow through porous media concept. Also eager are politicians and economists who see the importance of groundwater flows and various tertiary oil recovery processes. Use of flow through porous media was outlined by Bear [34] in his book. In his explanation of the pseudo transport coefficients of permeability, pressure gradients, and dispersion, Greenkorn [35] reviews the fundamentals of steady flow through porous media. Different kinds of difficulties relating to porous media were studied by Dwivedi et. al. [36], Devakar et. al [37], Gunnar and Hellström [38], Roy et. al. [39], and Chowdary et. al. [40].

The influence of magnetohydrodynamics on two-phase flow via a rectangular curved duct is not yet documented in the open literature, to the best of the author's knowledge. The objective of this study is to use a rectangular curved duct to introduce an external magnetic field into a two-phase, incompressible, unsteady flow in a porous medium. The Navier-Stokes equations and the level set equations with boundary conditions in the important in this era are solved using the finite element method. To understand the impact of the Hartmann number, radius of curvature, Dean number, aspect ratios, porosity, and particle concentration on each domain, the phase distribution, vector plot of the field flow (Dean vortex), velocity contour, and volume fraction of fluid on the domain are being shown for various times. Also compared are the results.

Mathematical Model

A laminar viscous incompressible unsteady three-dimensional two-phase flow is considered here. The flow passes through a curved duct with a rectangular cross-section as it flows through the porous medium. The length and width of the cross-section are $h(m)$ and $d(m)$,respectively. For consideration $h = 4m$ and $d = 4m$ are taken fixed for square duct. Let O indicate the duct's curvature's center and $L(m)$ indicate the radius of curvature shown in Fig.1. The analysis uses a mixture of water and Engine oil as the immiscible working fluid, which is sustained together into the curved duct path. In the curved channel inlet, Engine oil enters the outer domain, and water enters the

inner domain with different velocities. It is considered that though the inlet velocity is different the Reynolds number remains the same for the fluid in both domains. An uniform magnetic field B_0 is imposed into the outer domain of duct along the horizontal direction (X-direction). All physical properties of the assumed fluids are constant.

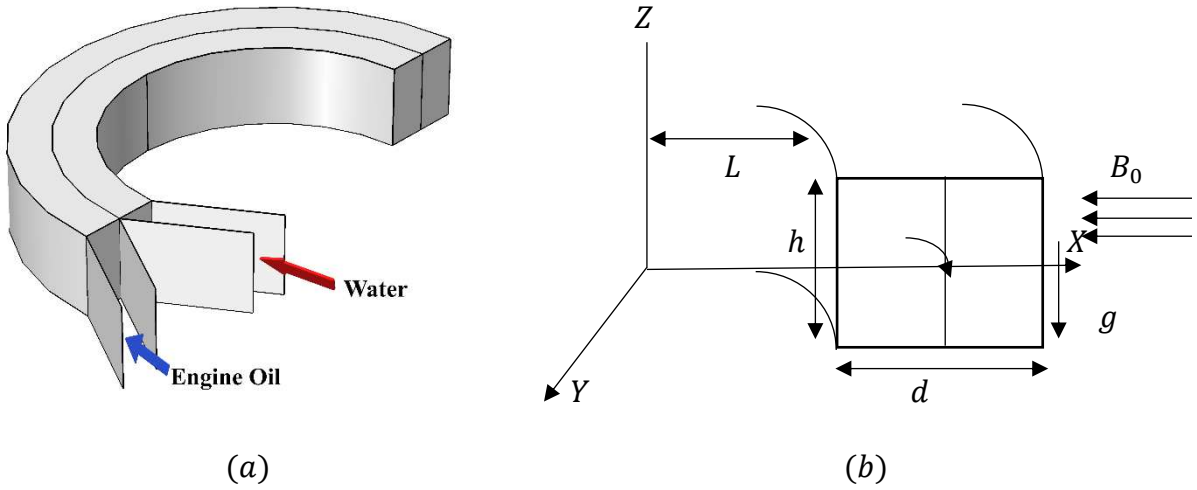

Fig. 1: (a) Co-ordinate system, (b) cross sectional view

The governing equations for the mathematical model are given by Kucuk [41] and Gyves [42] as follows:

Continuity equation:

$$\frac{\partial u}{\partial x}+\frac{\partial v}{\partial y}+\frac{u}{x+L}=0 \tag{1}$$

Momentum equations:

$$\frac{\partial u}{\partial t}+u\frac{\partial u}{\partial x}+v\frac{\partial u}{\partial y}-\frac{w^2}{x+L}=-\frac{1}{\rho}\frac{\partial P}{\partial x}+\nu\left[\frac{\partial^2 u}{\partial x^2}+\frac{\partial^2 u}{\partial y^2}+\frac{1}{x+L}\frac{\partial u}{\partial x}-\frac{u}{(x+L)^2}\right]-\frac{\mu u}{K}-\frac{\sigma {B_0}^2 u}{\rho} \tag{2}$$

$$\frac{\partial v}{\partial t}+u\frac{\partial v}{\partial x}+v\frac{\partial v}{\partial y}=-\frac{1}{\rho}\frac{\partial P}{\partial y}+\nu\left[\frac{\partial^2 v}{\partial x^2}+\frac{1}{x+L}\frac{\partial v}{\partial x}+\frac{\partial^2 v}{\partial y^2}\right]-\frac{\mu v}{K} \tag{3}$$

$$\frac{\partial w}{\partial t}+u\frac{\partial w}{\partial x}+v\frac{\partial w}{\partial y}+\frac{uw}{x+L}=-\frac{1}{\rho}\frac{1}{(x+L)}\frac{\partial P}{\partial z}+\upsilon\left[\frac{\partial^2 w}{\partial x^2}+\frac{\partial^2 w}{\partial y^2}+\frac{1}{x+L}\frac{\partial w}{\partial z}-\frac{w}{(x+L)^2}\right]-g \tag{4}$$

where $u, v,$ and w are velocity components in $x,\ y$ and z directions, respectively, ρ is density, ν is kinematic viscosity, σ is electrical conductivity, B_0 is external magnetic force (Lorentz force), L is radius of curvature and K is the porosity of the medium. The model neglects all terms of the order $\frac{1}{L}$ and $\frac{1}{L^2}$, except the centrifugal force term as in Gyves [43].

The boundary conditions at the channel and core walls and for inlet & outlet

$$(u, v, w) = 0 \qquad at\ r = L,\ r = L + d,\ \ h = 0, \text{and}\ \ h = h \tag{5}$$

$$\text{At the inlet-1} \qquad u = u_1\bar{n}$$

$$\text{and at the inlet-2} \qquad u = u_2\bar{n} \qquad \text{on the outlet } P = P_0 \tag{6}$$

The Dean number is typically denoted by

$$De = Re\left(\frac{d}{L}\right)^{1/2} \tag{7}$$

Where Re is the Reynolds number, d is a typical length scale associated with the channel cross-section, L is the radius of curvature of the path of the duct.

Where Reynolds number Re is defined by

$$Re = \frac{\rho dU}{\mu} \tag{8}$$

The Hartmann number is denoted by

$$Ha = B_0 L\sqrt{\frac{\sigma}{\mu}} \tag{9}$$

Where Ha is Hartmann number, B_0 is the magnetic field density, L is the radius of curvature of the path of the duct, σ is the electrical conductivity and μ is the dynamical viscosity.

Where ρ and μ are densicity and dynamical viscosity of the fluid. Since the governing equations are non-dimensional and ρ, d and μ are considred constant, so Dean number(De) as well as Reynolds number (Re) depand on value of u.

Porosity can be written as

$$K = \frac{V - V_s}{V} = \frac{V_p}{V} = \frac{Pore\ \ Volume}{Bulk\ Volume} \tag{10}$$

Where V is the bulk rock volume V that is not occupied by solid matter, V_s is volume of solid and $V_p = V - V_s$ is the pore volume.

The level set function $\emptyset$ can be represented by the following equation: Olsson et al [44].

$$\frac{\partial \emptyset}{\partial t} + \boldsymbol{u}.\nabla\emptyset = \gamma\nabla.\left(\varepsilon\nabla\emptyset - \emptyset(1-\emptyset)\frac{\nabla\emptyset}{|\nabla\emptyset|}\right) \tag{11}$$

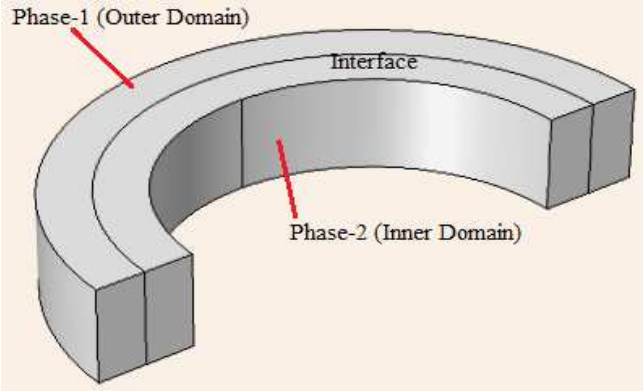

Fig. 2: Phase distribution

Where $\boldsymbol{u}$ is the fluid velocity. The ε parameter determines the thickness of the layer of the interface. The γ parameter determines the amount of reinitialization and $\emptyset$ is the level set function varies from zero to one. For Engine oil $\emptyset = 0$ and for water $\emptyset = 1$.

The level Set function $\emptyset$ is defined by

$$\emptyset(x) = \begin{cases} 0 & x \in phase - 1 \\ 1 & x \in phase - 2 \end{cases} \tag{12}$$

For calculating surface tension, the interface normal and curvature are obtained according to the sign function

$$\overline{n} = \frac{\nabla\emptyset}{|\nabla\emptyset|}\Big|_{\emptyset=0} \qquad \text{and} \qquad k = \nabla.\frac{\nabla\emptyset}{|\nabla\emptyset|}\Big|_{\emptyset=0} \tag{13}$$

The level set function is used to determine the density and dynamic viscosity globally by

$$\rho = \rho_{Eo} + (\rho_w - \rho_{Eo})\emptyset \tag{14}$$

$$\mu = \mu_{Eo} + (\mu_w - \mu_{Eo})\emptyset \tag{14}$$

where ρ_{Eo}, ρ_w, μ_{Eo} and μ_w are the density and dynamic viscosity of engine oil and water respectively.

Numerical Solution

The finite element method is a numerical technique used to solve the problem. To create a simulation, the entire structure must be divided into small elements, called mesh. Calculations are made for each individual element. Combining the individual results gives the final result of the structure. Among the elements that are taken, we know the values at certain points but not on each point. These 'fixed points' are

called nodal points and are often located at element boundaries. The finite element method formulation of a boundary value problem finally results in a system of algebraic equations. And the system of algebraic equation will be solved by matrix formula.

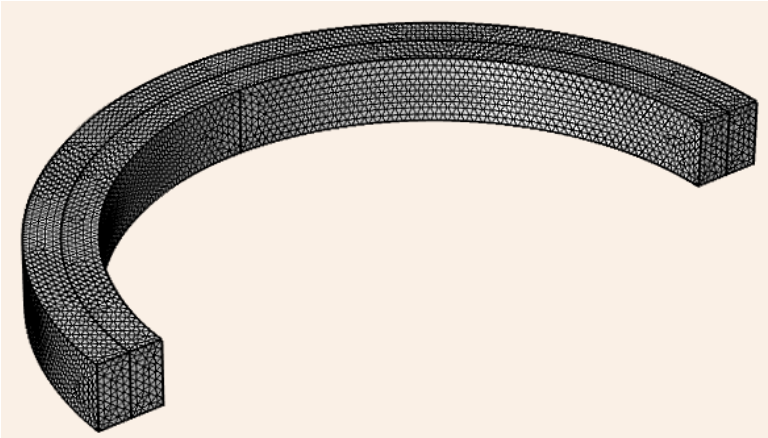

Fig. 3: Mesh generation of the 3D domain

The Finite element meshing of the computational Domain is displayed in Figure 3. A grid refinement test has been performed until the results show insignificant change for further refined mesh size.

Table 1: Element size comparison

Mesh Size	Extremely Coarse	Extra Coarse	Coarse	Coarser	Normal	Fine
Number of elements	2256	6448	18196	61314	131956	389530
Average Velocity	0.16343	0.17918	0.18732	0.19989	0.21281	0.21299

From the above Table-1, it is observed that results for average velocity magnitude have no significant change up to three decimal places for Normal and Fine mesh size. Therefore, Normal mesh size is chosen to find the grid independent solution and to save computational time.

Results and Discussion

Two-phase and single-phase fluids display fundamentally different flow behavior. Because their components may have different flow (slip) velocities and may not experience mass exchanges between phase boundaries, two-phase fluids display unusual flow dynamics. Consequently, the relative magnitudes of fluid component properties, in particular the density and viscosity, have an

effects on the flow behavior of non-mixing two-phase fluids. The centrifugal forces generated by the radius of curvature in a curved duct have a significant impact on the heavier fluid components. The distribution, deformation, phase interface area, and flow control in a fluid flow are mostly determined by such combined interactions.

Table 2: Thermo-physical properties of the different fluids as follows

Physical properties	Water (H_2O)	Engine oil (EO)	Kerosene	Ethylene glycol	Gasoline	Ethanol	Heptane
$C_p\ [Jkg^{-1}K^{-1}]$	4179	1880.3	2090	2417	2200	2440	2242
$\rho\ [Kgm^{-3}]$	997.1	888.23	780	110.7	714.6	790	684
$\kappa\ [Wm^{-1}K^{-1}]$	0.613	0.145	0.149	0.252	0.15	0.18	0.13
$\mu[Kgm^{-1}s^{-1}]$	0.001003	0.8541	0.00164	0.0162	0.006	1.194	0.389
$\sigma\ [s^{-1}]$	5.5×10^{-6}	23.004	6×10^{-10}	0.256	2.5×10^{-5}	0.554	3 x 10^{-2}

The magnetohydrodynamic effect on unsteady laminar incompressible two-phase fluid flow in a porous medium through a three-dimensional rectangular curved channel is shown here.The results in terms of phase distribution, axial flow velocity, velocity contour and vector plot of flow field have been discussed for the various radius of curvature ($20m \leq L \leq 100m$) and compared with $200m$, Dean number ($45 \leq De \leq 1800$), aspect ratio (1:1 to 1:6), particle concentration of outer domain ($0.0 \leq \emptyset \leq 1$) and several time steps (0s to 300s). Also, six different fluids (Engine Oil, Kerosene, Ethylene glycol, Heptane, Gasoline, Ethanol) have been tested in the outer domain. All the figures are taken at the cut plane of YZ-plane at $x = 0$.

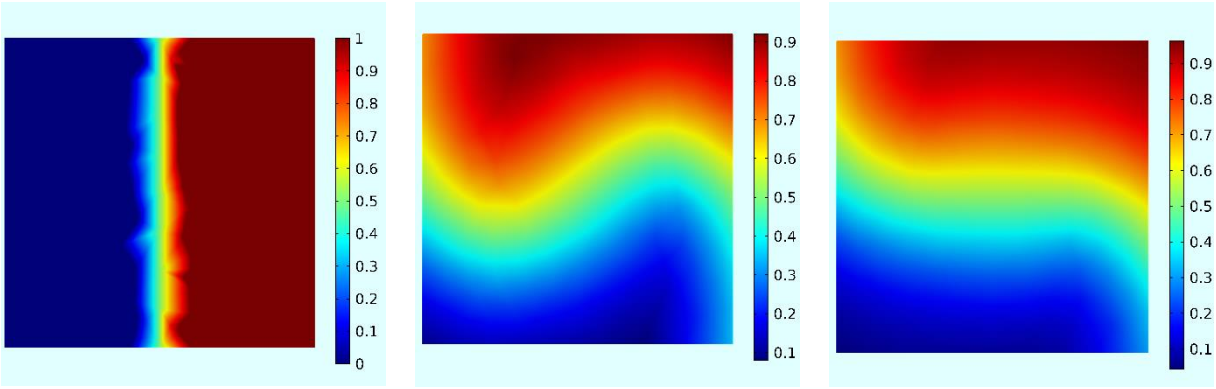

t = 0^{th}s t = 60^{th}s t = 120^{th}s

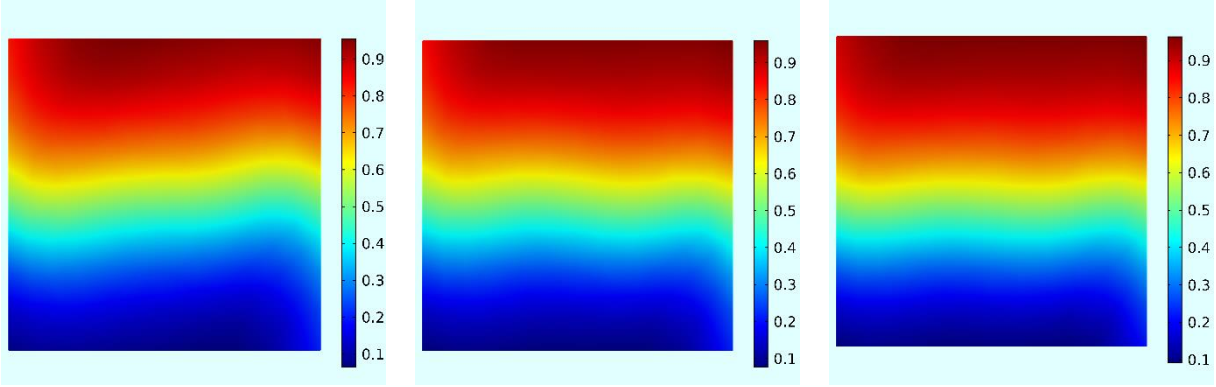

$t = 180^{th}s$ $t = 240^{th}s$ $t = 300^{th}s$

Fig. 4(a): Volume fraction visualization at different time. When $De = 180, Ha = 1, L = 20m$ and $\emptyset = 0.0$ at outer domain for aspect ratio (1:1).

Volume fraction visualization at different moments is shown in Fig. 4(a). The multiphase fluid was located in a different domain at time $t = 0^{th}s$. Water enters the inner domain (red), engine oil enters the outer domain (blue), and yellow denotes the domain interface. The multiphase flow will be mixed after a little time. Low viscosity fluid will be positioned at the top, with high viscosity fluid positioned at the bottom. It was also noted that the interface will become periodic at times $t = 60^{th}s$ and $120^{th}s$ and that the mixed fluid will reach steady state at time $t \geq 300^{th}s$.

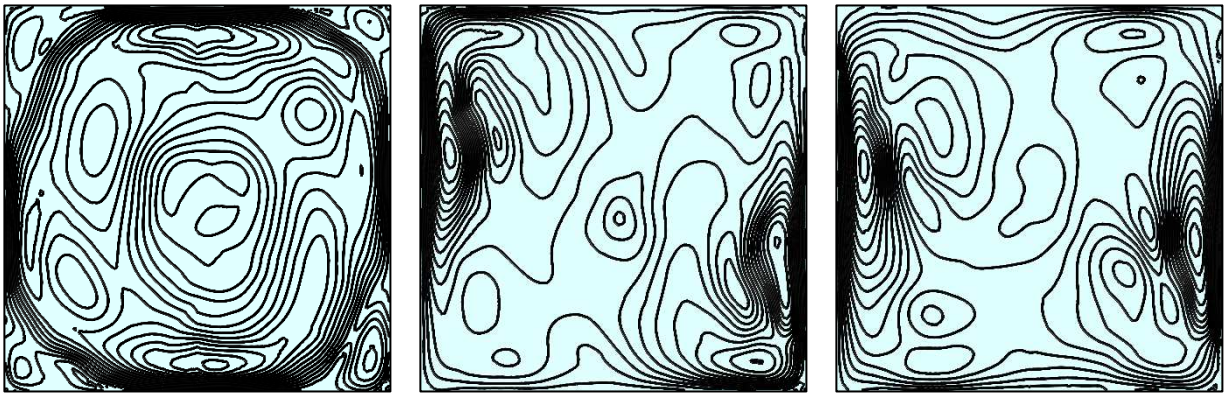

$t = 60^{th}s$ $t = 120^{th}s$ $t = 150^{th}s$

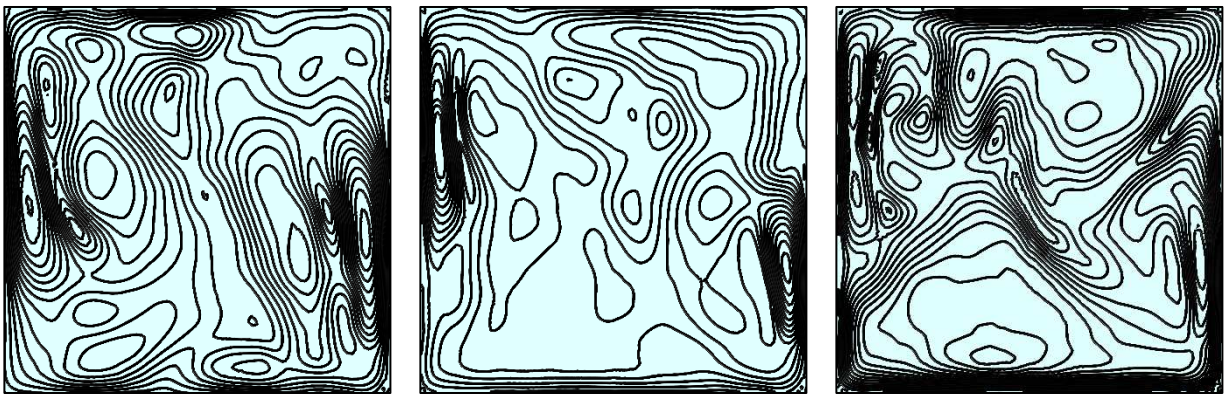

$t = 180^{th}s$ $t = 240^{th}s$ $t = 300^{th}s$

Fig. 4(b): Velocity contour at different time. When $De = 180, Ha = 1, L = 20m$ and $\emptyset = 0.0$ at outer domain for aspect ratio (1:1).

The velocity contour of the flow is depicted in Fig.4(b). When eight additional contours were shown inside the main vortex, which is located in the upper part of the duct cross-section, at time $t = 60^{th}s$, it is concluded that the Dean's flow is in rotational form. At time $t = 120^{th}s$, $150^{th}sand\ 240^{th}s$,there are ten contours, and it also manifests the axial flow shift at the duct's inner and outer walls. Dean's flow has grown erratic as a result. But when time $t = 180^{th}s\ and\ 300^{th}s$,there are twelve to fourteen contours, which also demonstrate the dispersed axial flow in both domains. That's why Dean's flow is likewise disorganized.

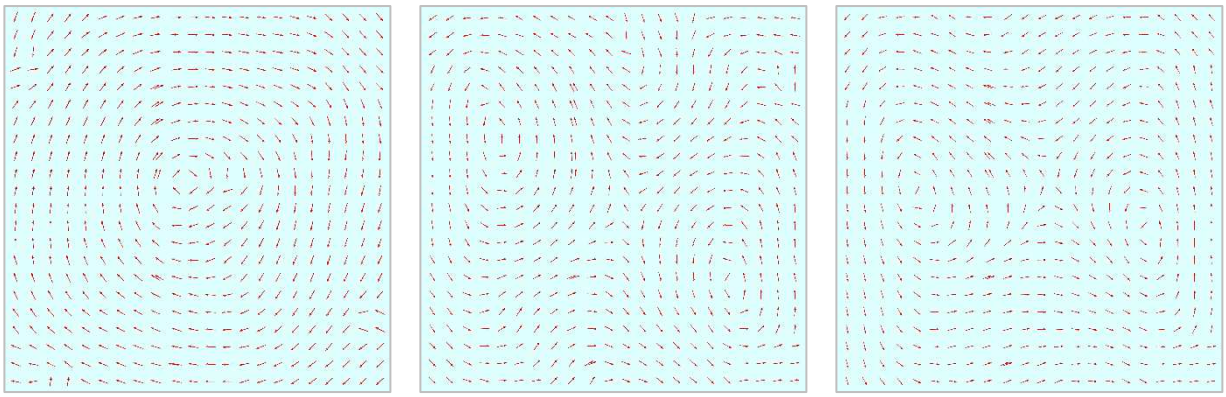

$t = 60^{th}s$ $t = 120^{th}s$ $t = 150^{th}s$

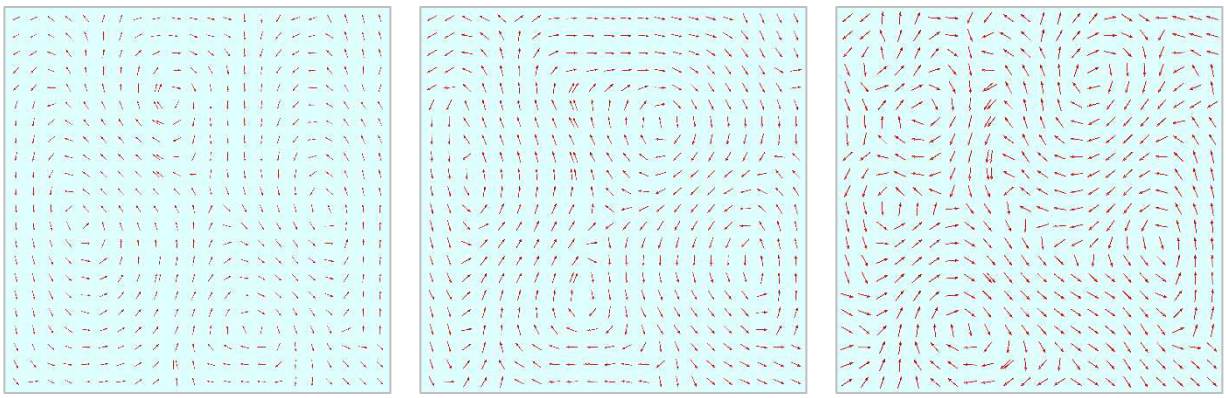

$t = 180^{th}s$ $t = 240^{th}s$ $t = 300^{th}s$

Fig. 4(c): Vector plot of flow field (Dean vortex) at different time. When $De = 180, Ha = 1, L = 20$ and $\emptyset = 0.0$ at outer domain for aspect ratio (1:1).

A vector plot of the flow field is displayed in Fig. 4(c). One Dean vortex of solution is seen to be centered in the duct's center at time $t = 60^{th}s$ s. At time $t = 120^{th}s$ and $150^{th}s$,there are two Dean vortices of secondary flow patterns in addition to a few parallel lines all along wall. The adjacent vortices are moving in opposing directions. Four Dean vortices of solution for secondary flow are present at time $t = 180^{th}s$ and $240^{th}s$. And the directions of each pair of vortexes are reversed. Furthermore, six symmetric Dean vortices and two symmetric vortex solutions with opposite directions are visible at time $t \geq 300^{th}s$.

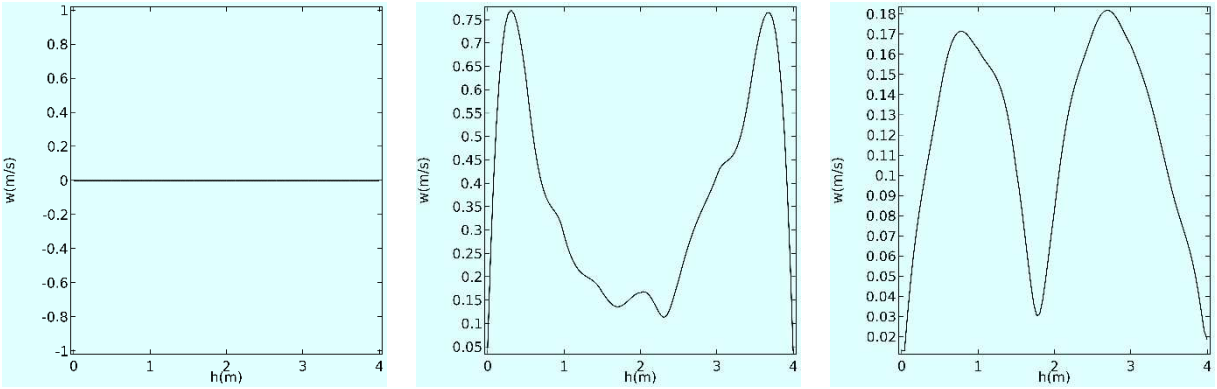

$t = 0^{th}s$ $t = 60^{th}s$ $t = 120^{th}s$

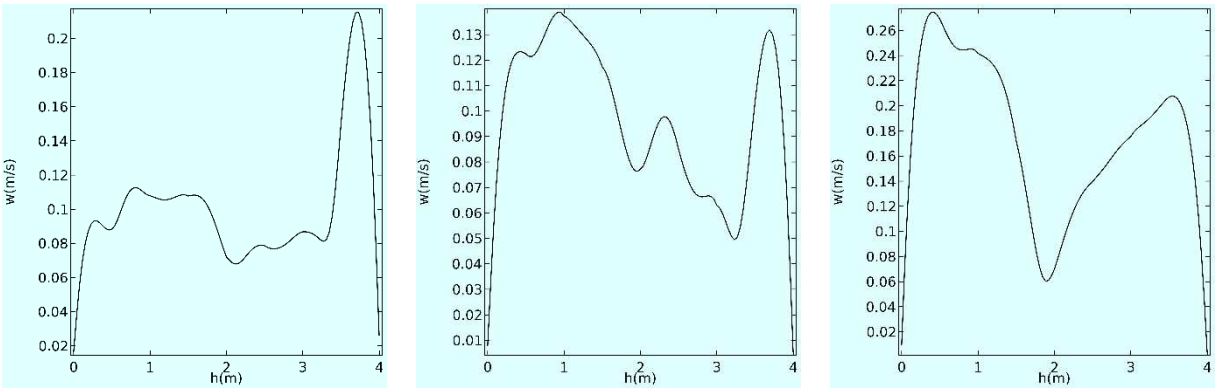

$t = 180^{th}s$ $t = 240^{th}s$ $t = 300^{th}s$

Fig. 4(d): Axial flow velocity at different time. When $De = 180, Ha = 1, L = 20m$ and $\emptyset = 0.0$ at outer domain. For aspect ratio (1:1).

Fig. 4(d) demonstrates that the axial flow velocity is in a straight line at time $t = 0^{th}s$ because there is no velocity at this point. Axial flow velocity of mixed fluid exhibits a hyperbolic shape and multiple orbits at times $t = 60^{th}s$ and $120^{th}s$, having low viscosity fluid flowing at a greater rate than high viscosity fluid. Moreover, it has been observed that the axial flow velocity of mixed fluid has a curved line shape at times $t = 180^{th}s$ and that the velocity of high viscosity fluid is higher than that of low viscosity fluid. However, at $t = 240^{th}s$, the axial flow velocity of the mixed fluid is curved and the velocity of the low viscosity fluid is larger than that of the velocity of the high viscosity fluid. Finally, when t=300 s, the axial flow velocity of a mixed fluid is hyperbolic and only generates two orbits, the velocity of low viscosity fluid is larger than that of high viscosity fluid.

Figure 4(e) depicts the phase distribution at various locations. Phase 1 (heavier fluid/engine oil), which is seen to be in dynamic equilibrium at the this center, is surrounded by Phase 2 (light fluid/water) in the cross section at $t = 60^{th}s$. Further, extended centrifugal forces are applied to the fluid mixture. At time $t = 120^{th}s, 150^{th}s, 180^{th}s\ and\ 240^{th}s$, Phase 1 is visible attached adjacent to the outer and inner walls, whereas Phase 2 is spread in the center. Again, at $t = 300^{th}s$, Phase 1 is visible close to the upper and lower wall, while Phase 2 is visible close to the outside and inner wall.

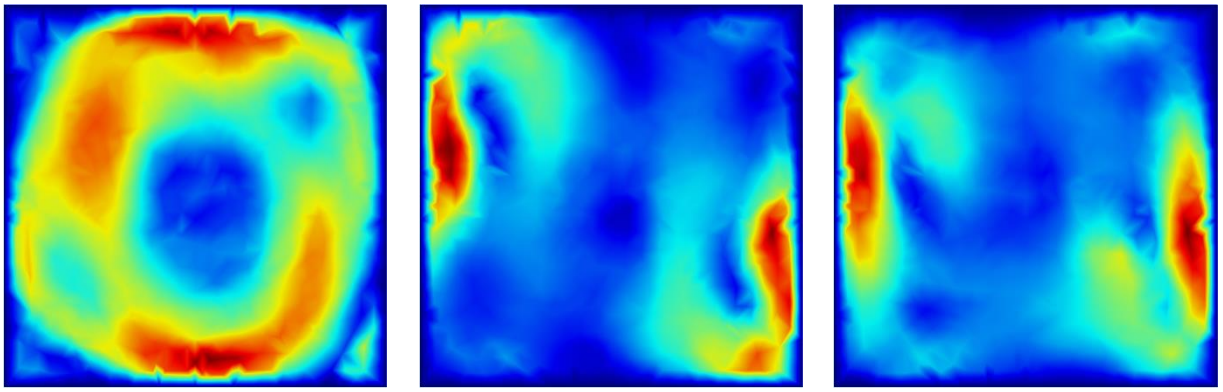

$t = 60^{th}s$ $t = 120^{th}s$ $t = 150^{th}s$

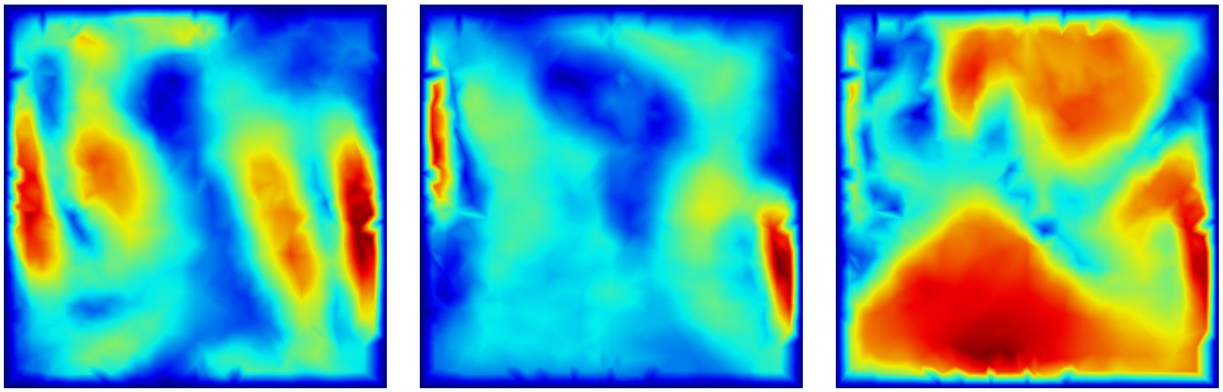

$t = 180^{th}s$ $t = 240^{th}s$ $t = 300^{th}s$

Fig. 4(e): Phase distribution at different time. When $De = 180, Ha = 1,\ L = 20m$ and $\emptyset = 0.0$ at outer domain for aspect ratio (1:1).

Effects of the Hartman number on the velocity contour depicted in fig. 5(a). There are sixteen to eighteen contours and the axial flow is shifted close to the duct's outer wall as depicted in the figure when $Ha = 1{,}100\ and\ 500$. Thus, Dean flow is chaotic.

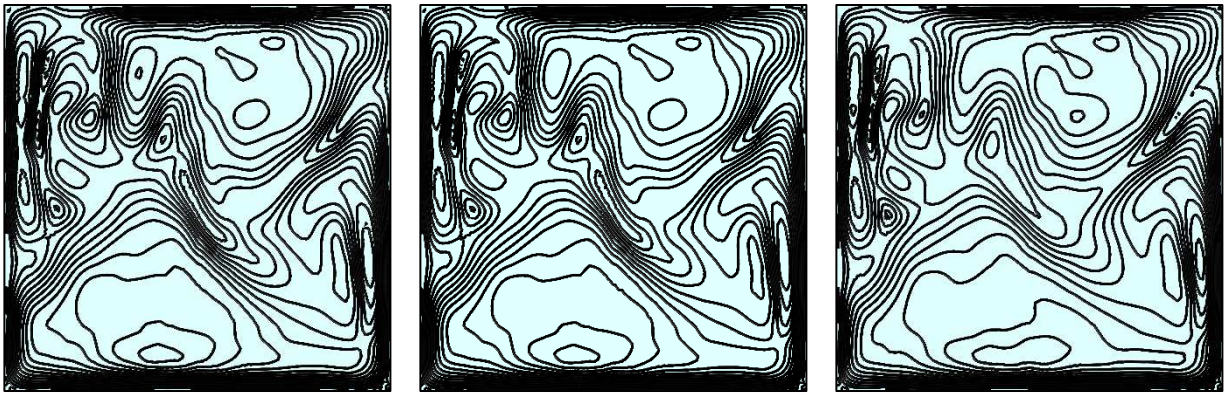

$Ha = 1$ $Ha = 100$ $Ha = 500$

Ha = 1000 Ha = 1500 Ha = 2000

Fig. 5(a): Effect of Hartmann number on velocity contour. When L = 20m, De = 180, t = 300^{th}s and ∅ = 0.0 at outer domain for aspect ratio (1:1).

Again It's also visible that there are twelve to fourteen contours and that the axial flow is displaced close to the duct's outer wall when the Hartmann number $Ha = 1000, 1500\ and\ 2000$. Thus, Dean's flow is also chaotic.

Effect of Hartmann number on vector plot of flow field is shown in Fig. 5(b). There are six symmetric Dean vortex vortexes and each pair is moving in the opposite direction when the Hartmann number $Ha = 1,500\ and\ 1000$. However, there are eight Dean vortex solution for secondary flow, and each pair of vortex is moving in the opposite direction, according to Hartmann number $Ha = 1000, 1500\ and\ 2000$.

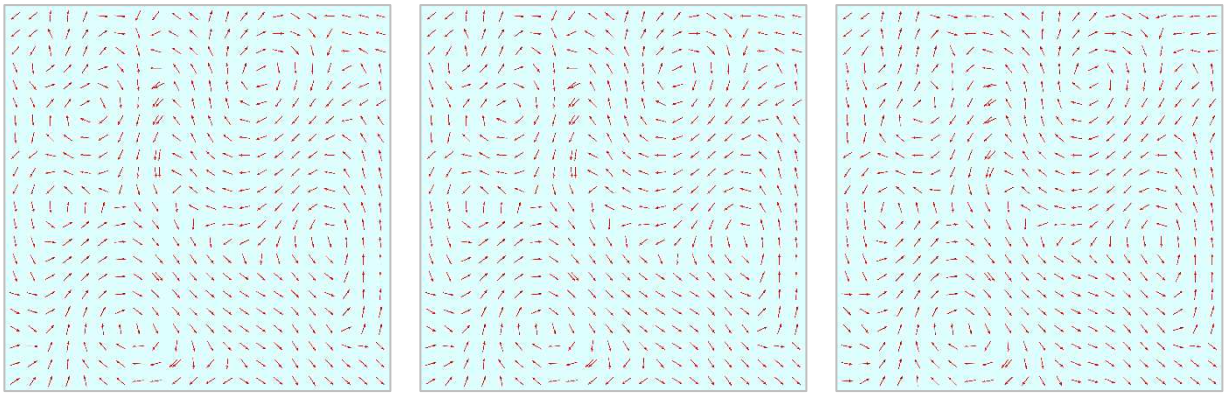

Ha = 1 Ha = 100 Ha = 500

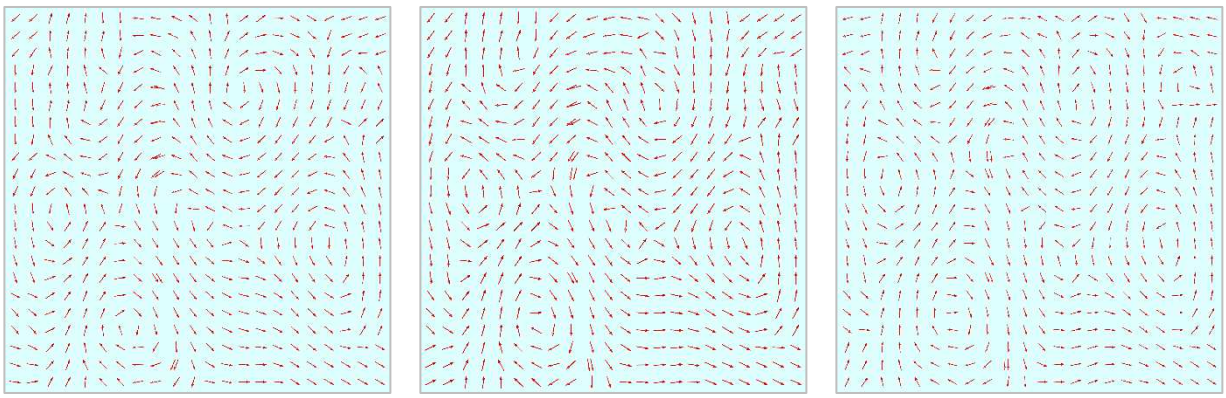

Ha = 1000 Ha = 1500 Ha = 2000

Fig. 5(b): Effect of Hartmann number on vector plot of flow field. When L = 20m, De = 180, t = 300^{th}s and $\emptyset = 0.0$ at outer domain and for aspect ratio (1:1).

Fig. 5(c) displays Hartmann numbers effect on axial flow velocity. For $Ha = 1,500\ and\ 1000$, the axial flow velocity of the combined fluid is hyperbolic and produces multiple orbits.

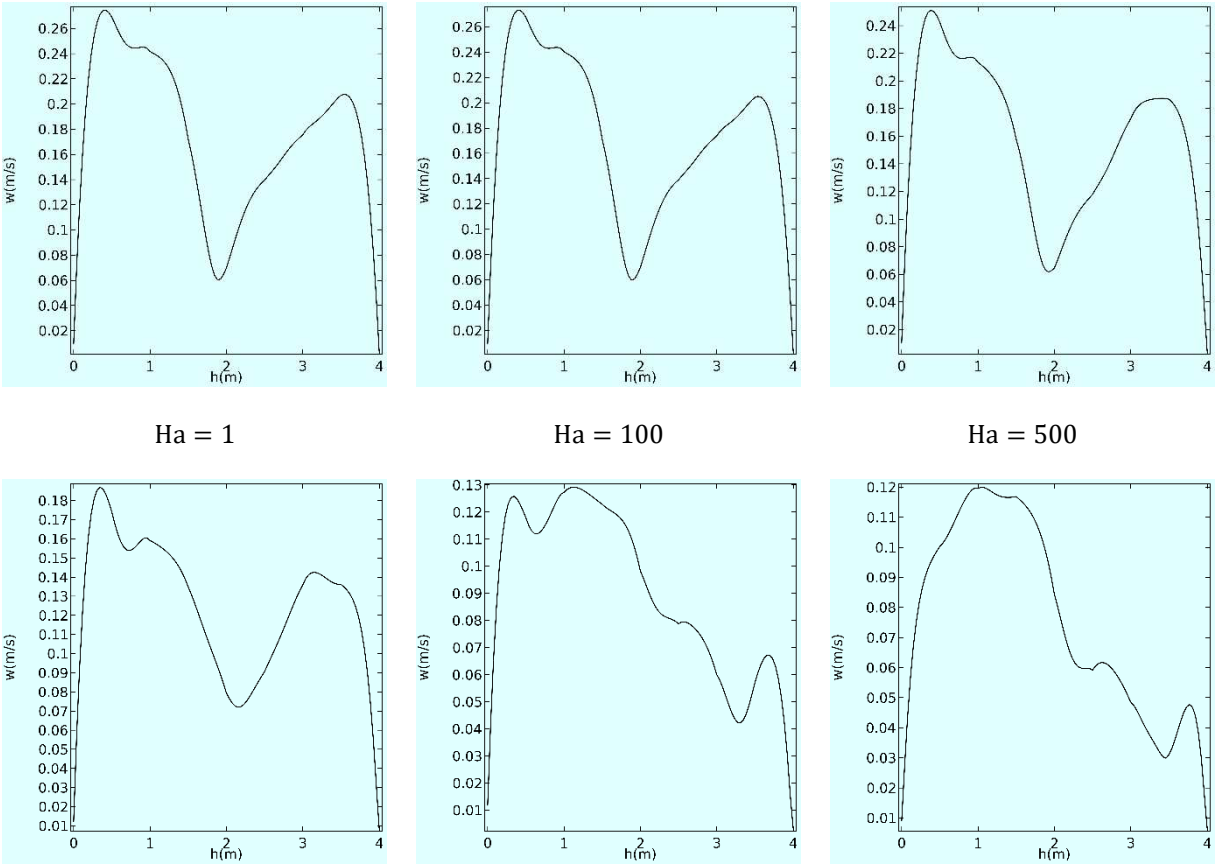

Ha = 1 Ha = 100 Ha = 500

Ha = 1000 Ha = 1500 Ha = 2000

Fig. 5(c): Effect of Hartmann number on axial flow velocity. When L = 20m, De = 180, t = 300^{th}s and $\emptyset = 0.0$ at outer domain an for aspect ratio (1:1).

Additionally, shows that high viscosity fluid flows with a higher velocity than low viscosity fluid. Again, when $Ha = 1000{,}1500\ and\ 2000$, the axial flow velocity is in the shape of a curve line as well as the velocity of a high viscosity fluid is higher than that of the low viscosity fluid.

Fig. 5(d) shows that the phase distribution for the effect of Hartmann number. Phase 1 (heavier fluid/engine oil) is found to reside in dynamic equilibrium in the upper and lower wall when Hartmann numbers $Ha = 1{,}100\ and\ 500$, whereas Phase 2 (light fluid/water) is seen to be spread all through the entire duct. However, Phase 1 (heavier fluid/engine oil) is found to reside in dynamic equilibrium on the lower wall and Phase 2 (light fluid/water) on the top portion of the duct when Hartmann number $Ha = 1000{,}1500\ and\ 2000$.

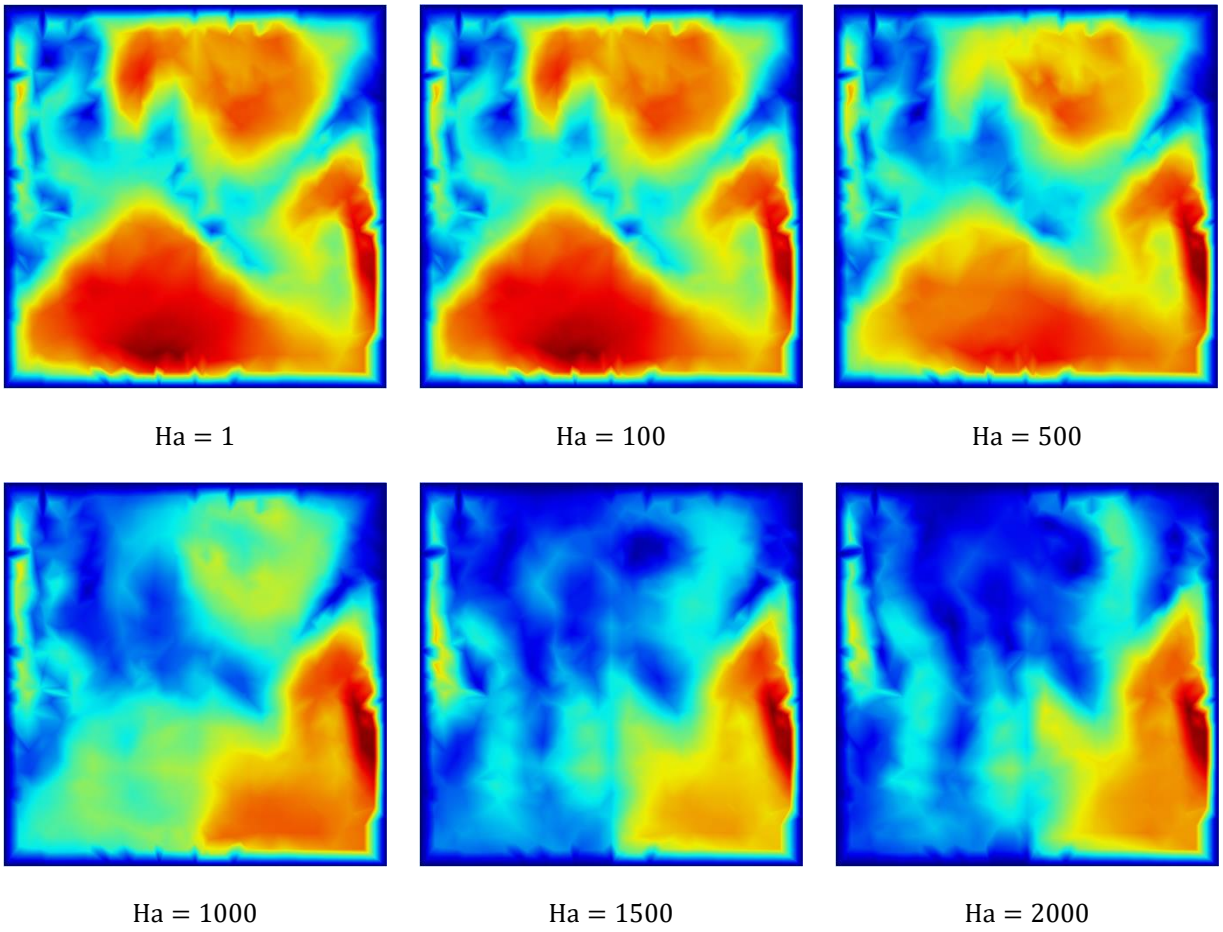

Fig. 5(d): Effect of Hartmann number at Phase distribution. When $L = 20m, De = 180, \emptyset = 0.0$ at time $t = 300^{th}s$ at outer domain for aspect ratio (1:1).

Fig.6(a) displays the effect of the radius of curvature on the velocity contour. There are fourteen contours and axial flow is shifted closer to the duct's outer wall when the radius of the curvature

$L = 20m$. Furthermore, there are eight contours at $L = 40m\ and\ 60m$, which also demonstrates that the axial flow is shifted closer to the duct's outer wall. Dean's flow is also chaotic under this aspect. Again, at $L = 80m$, contours have a tendency to congregate in the centers, and at $L = 100m$, four additional contours seem as inside the principal contour, all of which are positioned in the upper region of the duct cross-section. These suggest that the Dean's flow is transitioning to a steady state. Finally, all additional contours disappear when the radius of curvature is $L = 200m$, and only one principal contour exists. It suggests that behavior of the duct is shifting to resemble that of a straight closed channel or duct.

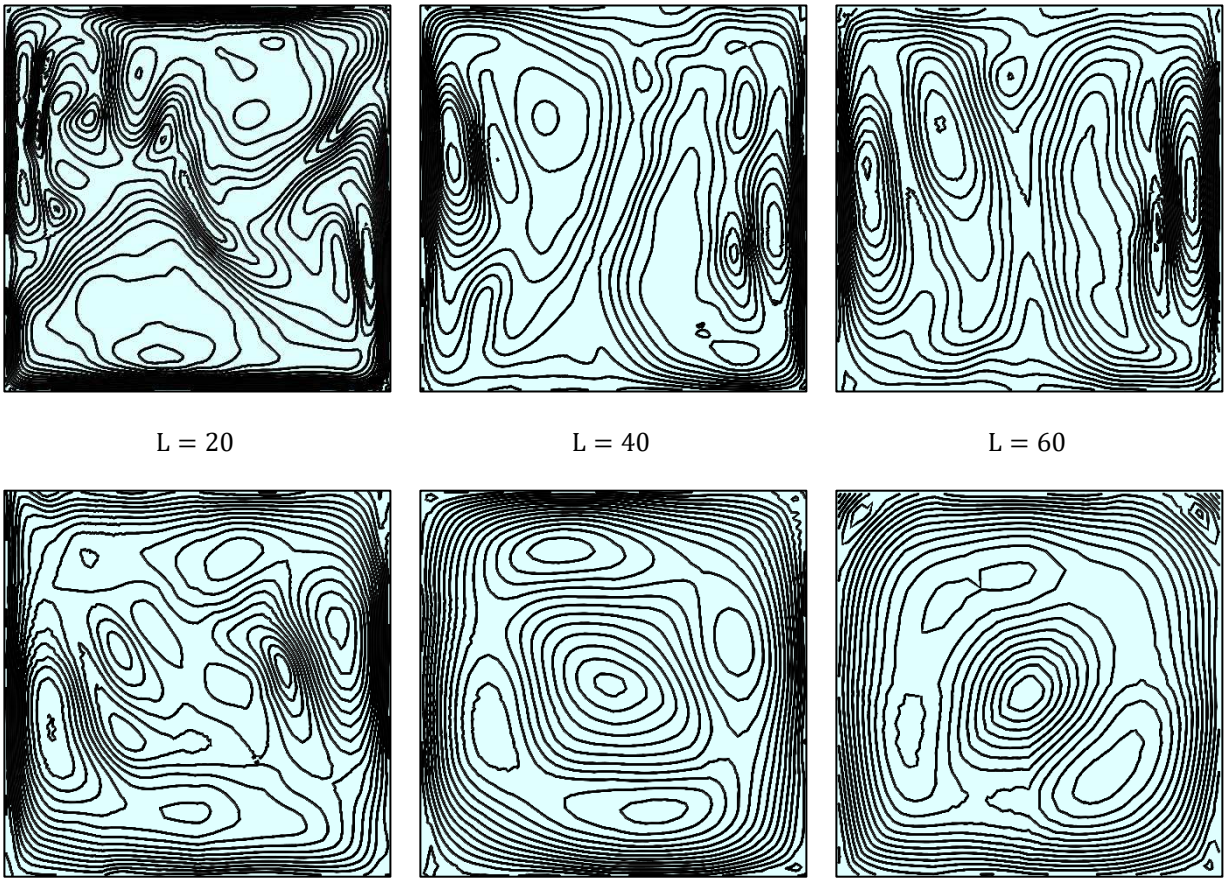

Fig. 6(a): Effect of radius of curvature on velocity contour. When $\mathrm{De} = 180,\ \mathrm{Ha} = 1, \mathrm{t} = 300^{th}\mathrm{s}$ and $\emptyset = 0.0$ at outer domain for aspect ratio (1:1).

The impact of the radius of curvature on the vector plot of the flow field is depicted in Fig. 6(b). There have been six symmetric Dean vortex solutions for secondary flow at $L = 20m\ and\ 40m$. Each pair of vortices is moving in the opposite direction. There are four asymmetric Dean vortex

solutions at $L = 60m$ and two symmetric Dean vortex solutions at $L = 80m$ for secondary flow. Additionally, the directions of each pair of vortexes are reversed. However, there is only one Dean vortex solution at $L = 100m$. It is also say that when $L \geq 100m$, vortex are found to oscillate on the centerline. Which shows that the flow behavior will change to resemble a parallel channel. Finally, there isn't any vortex solution when $L = 200m$.

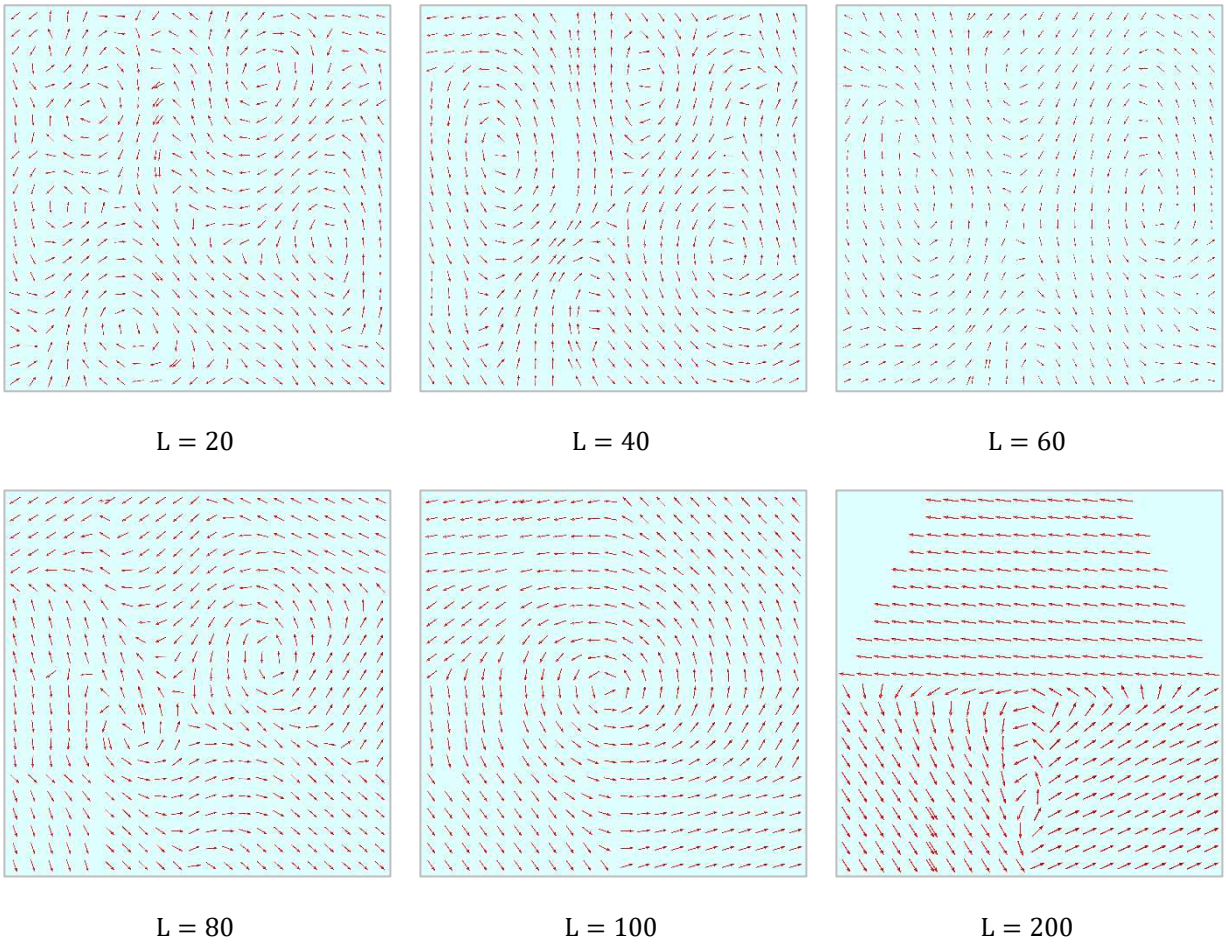

Fig. 6(b): Effect of radius of curvature on vector plot of flow field (Dean vortex). When De = 180, Ha = 1, t = 300^{th}s and ∅ = 0.0 at outer domain for aspect ratio (1:1).

The impact of radius of curvature on axial flow velocity is depicted in fig.6(c). When $L = 20m$, the mixed fluid's axial flow velocity assumes on a hyperbolic shape, generating multiple orbits, and the velocity of a high viscosity fluid is higher than that of the velocity of a low viscosity fluid. When $L = 40m$, the axial flow velocity of the mixed fluid takes the shape of a hyperbola, creating two orbits, with the velocity of the low viscosity fluid being higher than the high viscosity fluid. It was also noted that when $L = 60m$, the axial flow velocity of the mixed fluid has the shape of

a curve line and that the velocity of a low viscosity fluid is greater than that of the high viscosity fluid. Once again, at $L = 80m$, the axial velocity of a mixed fluid takes on a hyperbolic shape, creating multiple orbits, as well as the velocity of the high viscosity fluid is higher than that of the low viscosity fluid. Therefore, when $L = 100m\ and\ 200m$, the axial flow velocity is hyperbolic with two orbits, and indeed the velocity of a low viscosity fluid is greater than that of the high viscosity fluid.

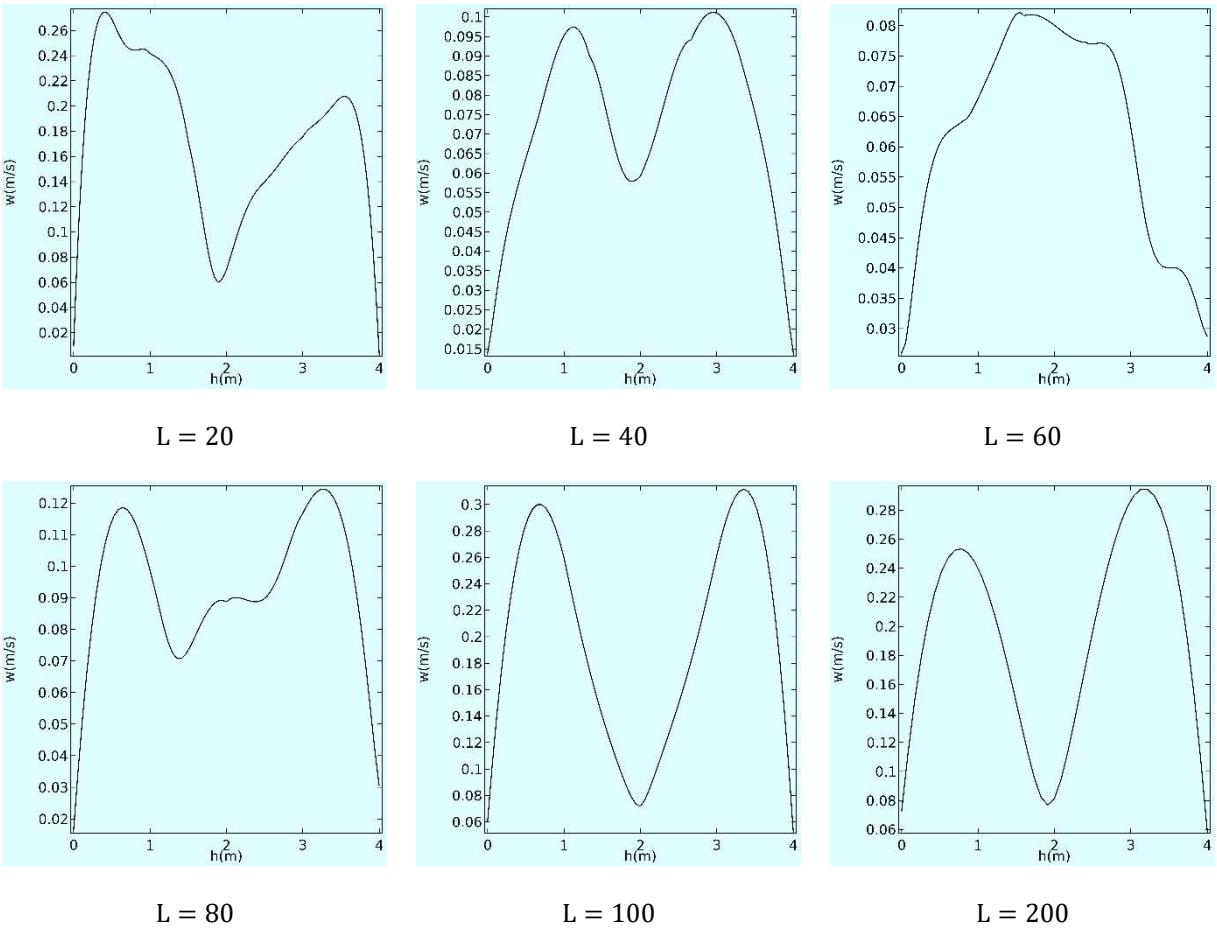

Fig. 6(c): Effect of radius of curvature on axial flow velocity. When $\mathrm{De} = 180, \mathrm{Ha} = 1,\ \mathrm{t} = 300^{th}\mathrm{s}$ and $\emptyset = 0.0$ at outer domain. For aspect ratio (1:1).

The phase distribution for the influence of radius of curvature is depicted in Fig. 6(d). When the radius of curvature is $L = 20m$, Phase 1 (the heavier fluid/engine oil) is seen to be in dynamic equilibrium in the top and bottom wall, whereas Phase 2 (the lighter fluid/water) is seen to be spread throughout the whole duct. When the radius of curvature is $L = 40m\ and\ 60m$,, Phase 1 is shown to be in dynamic equilibrium between the upper and lower walls, and Phase 2 is found to be in the middle between the both. However, phase 1 is seeking to gather at the cross section's center. When $L = 80m$,, while phase 2 is on either side

of it. Eventually, phase 1 was shown to be in dynamic equilibrium at $L = 100m\ and\ 200m$, with phase 2 surrounding it in the cross section's center.

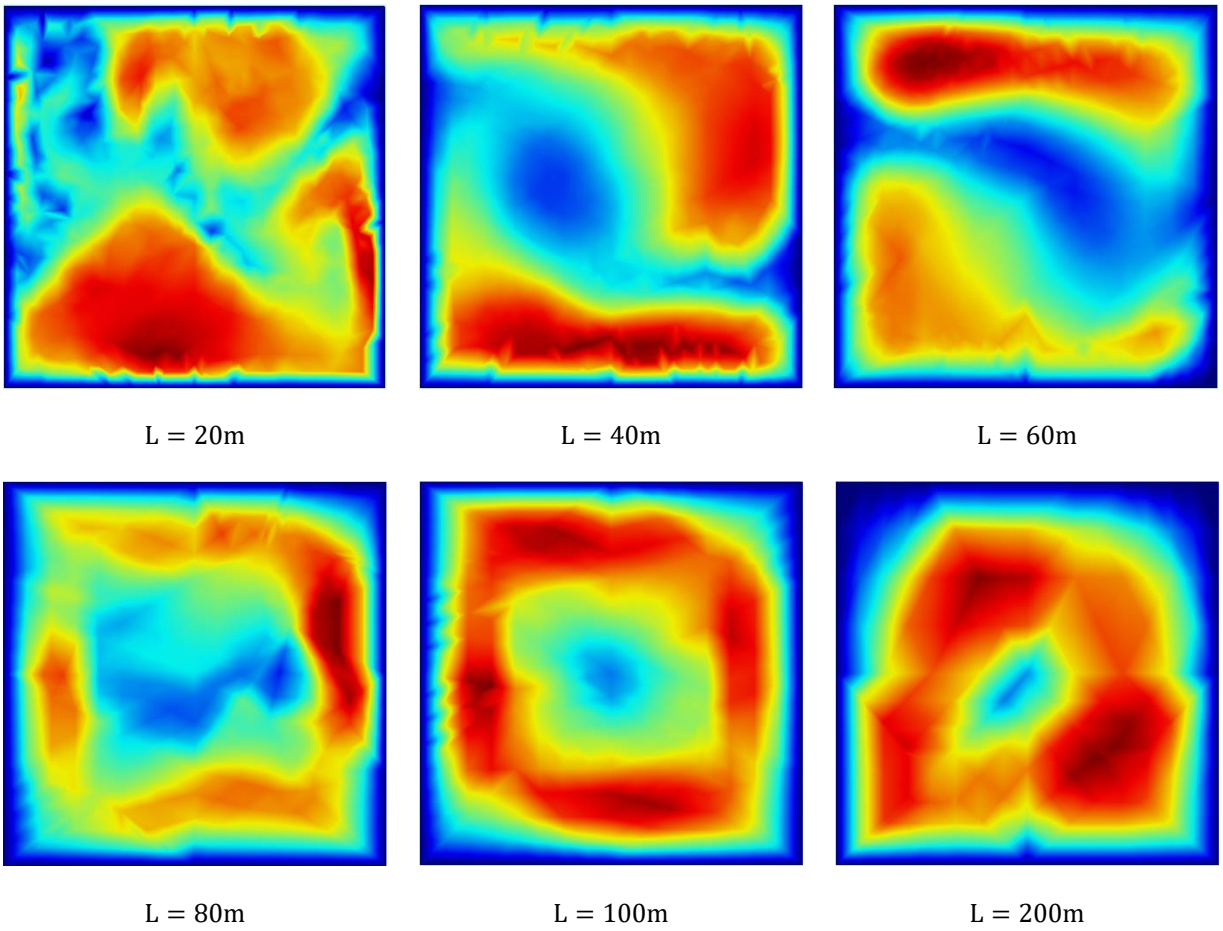

Fig. 6(d): Effect of radius of curvature at Phase distribution. When De = 180, Ha = 1, $\emptyset = 0.0$ at time t = 300^{th}s at outer domain for aspect ratio (1:1).

Fig. 7(a) displays the effect of the Dean number on the velocity contour. There are ten to twelve contours and axial flow is shifted closer to the duct's outer wall when the Dean number $De = 45\ and\ 180$. So, Dean's flow is chaotic. Furthermore, there are two to four contours at $De = 540\ and\ 900$, which also demonstrates that the axial flow is shifted closer to the duct's outer wall. Dean's flow is also chaotic under this aspect. It is noted that there are only two contours at $De = 1440\ and\ 1800$, which also show that the axial flow is shifted near to the inner duct's wall. These suggest that the Dean's flow is transitioning to a steady state.

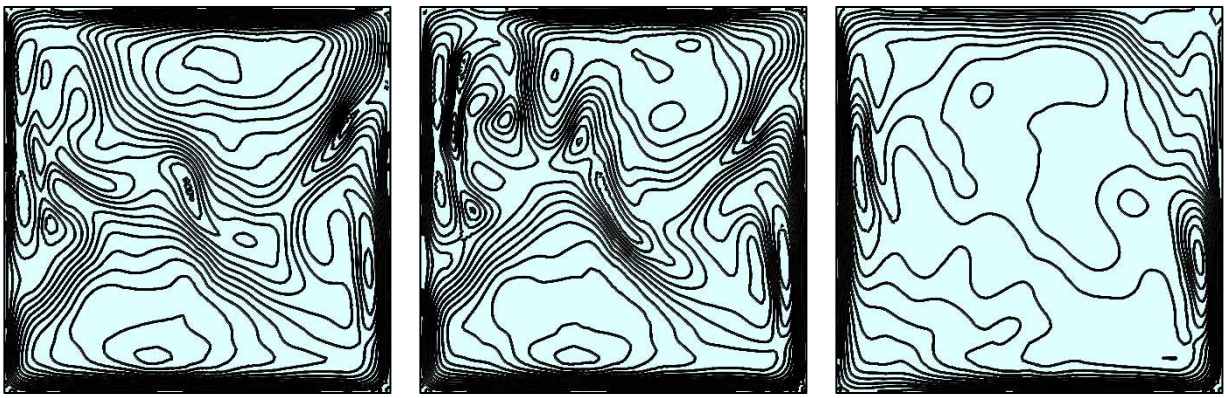

De = 45 De = 180 De = 540

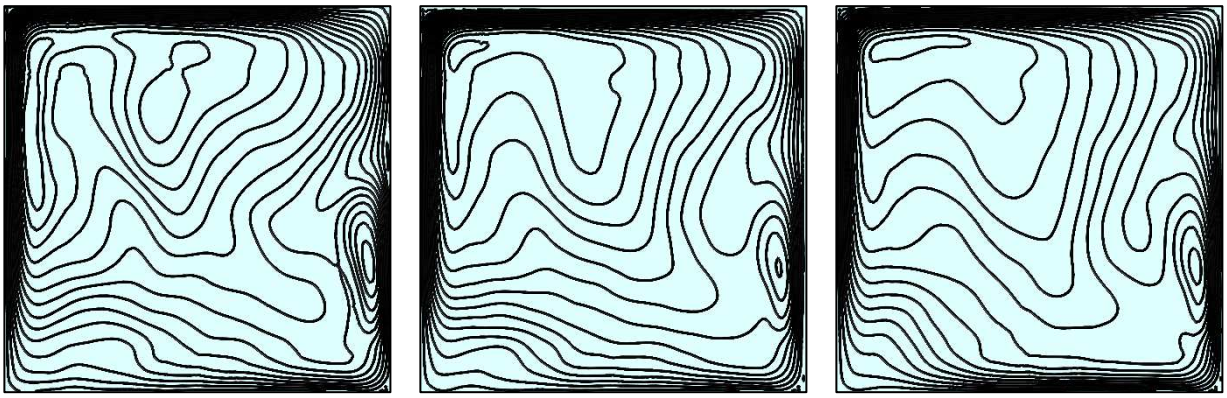

De = 900 De = 1440 De = 1800

Fig. 7(a): Effect of Dean number on velocity contour. When L = 20m, Ha = 1, t = 300^{th}s and ∅ = 0.0 at outer domain for aspect ratio (1:1).

The impact of the Dean number on the vector plot of the flow field is depicted in Fig. 7(b). There have been six symmetric Dean vortex solutions for secondary flow at $De = 45, 180, 540 \; and \; 900$. Each pair of vortices is moving in the opposite direction.

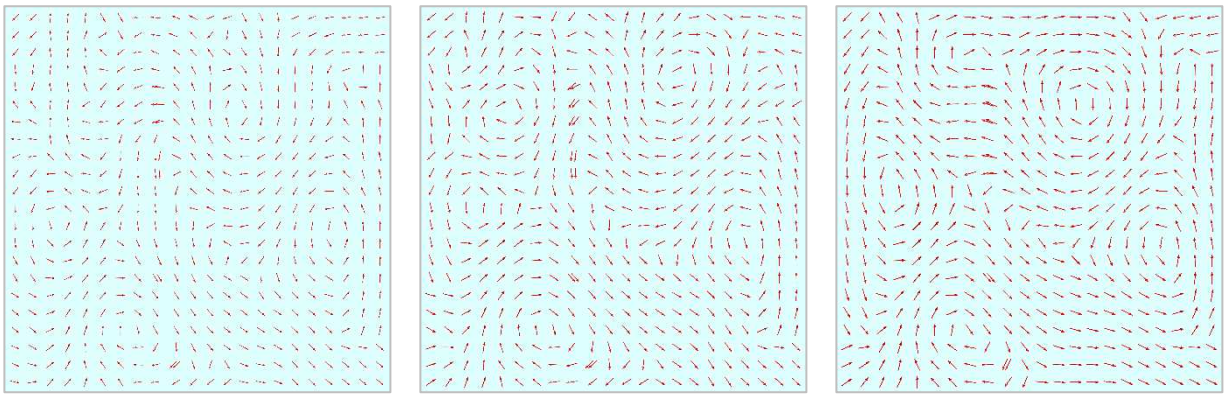

De = 45 De = 180 De = 540

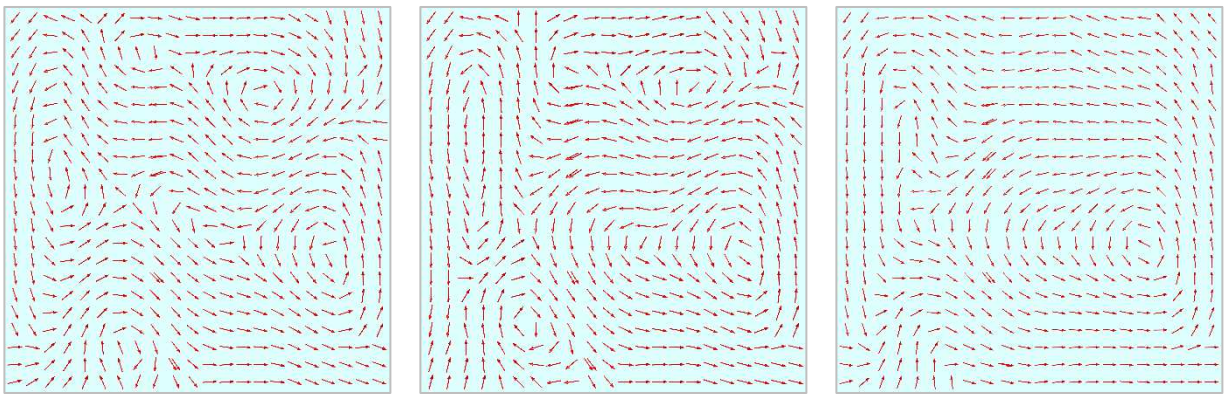

De = 900 De = 1440 De = 1800

Fig. 7(b): Effect of Dean number on vector plot of flow field (Dean Vortex). When L = 20m, Ha = 1, t = 300^{th}s and $\emptyset = 0.0$ at outer domain and for aspect ratio (1:1).

Furthermore, there are two symmetric Dean vortex solutions for secondary flow for $De = 1440$. Each pair of vortices is moving in the opposite direction. However, there is only one Dean vortex solution with some parallel line along the wall at $D = 1800$.

Fig. 7(c) illustrated the effect of Dean number on axial flow velocity. When $De = 45\ and\ 180$, the mixed fluid's axial flow velocity assumes on a hyperbolic shape, generating multiple orbits, and the velocity of a low viscosity fluid is higher than that of the velocity of a high viscosity fluid for $De = 45$ but for $De = 180$, the velocity of a high viscosity fluid is higher than that of the velocity of a low viscosity fluid. Moreover, it has been observed that the axial flow velocity of mixed fluid has multiple small curved line shape at times $De = 540$ and that the velocity of high viscosity fluid is higher than that of low viscosity fluid.

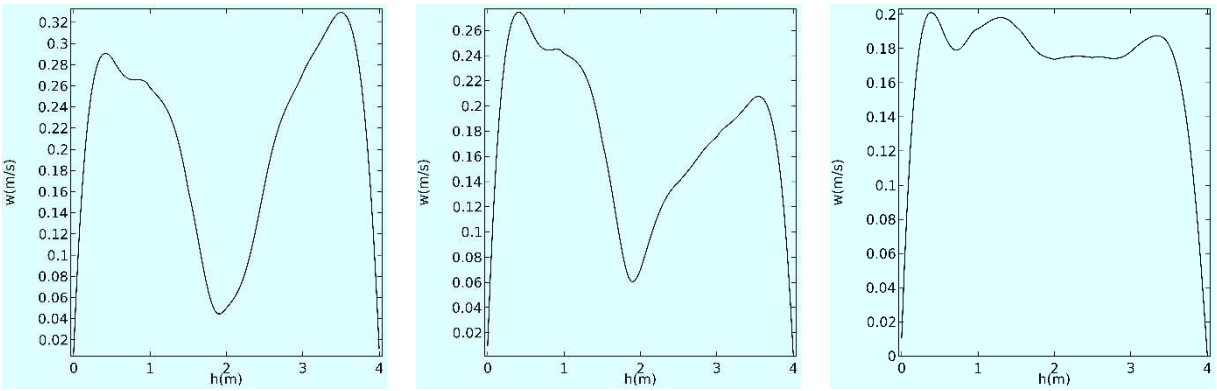

De = 45 De = 180 De = 540

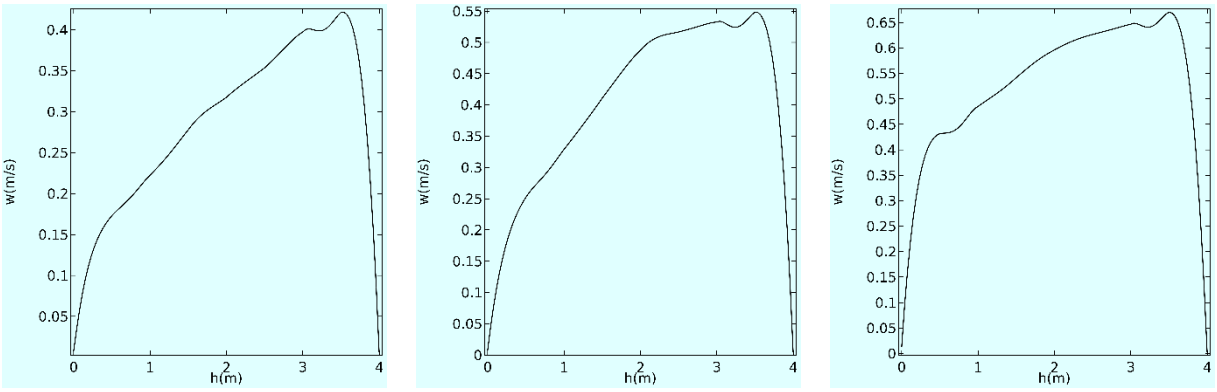

De = 900 De = 1440 De = 1800

Fig. 7(c): Effect of Dean number on axial flow velocity. When L = 20m, Ha = 1, t = 300^{th}s and ∅ = 0.0 at outer domain an for aspect ratio (1:1).

However, at $De = 900,1440\ and\ 1800$, the axial flow velocity of the mixed fluid is curved and the velocity of the low viscosity fluid is larger than that of the velocity of the high viscosity fluid.

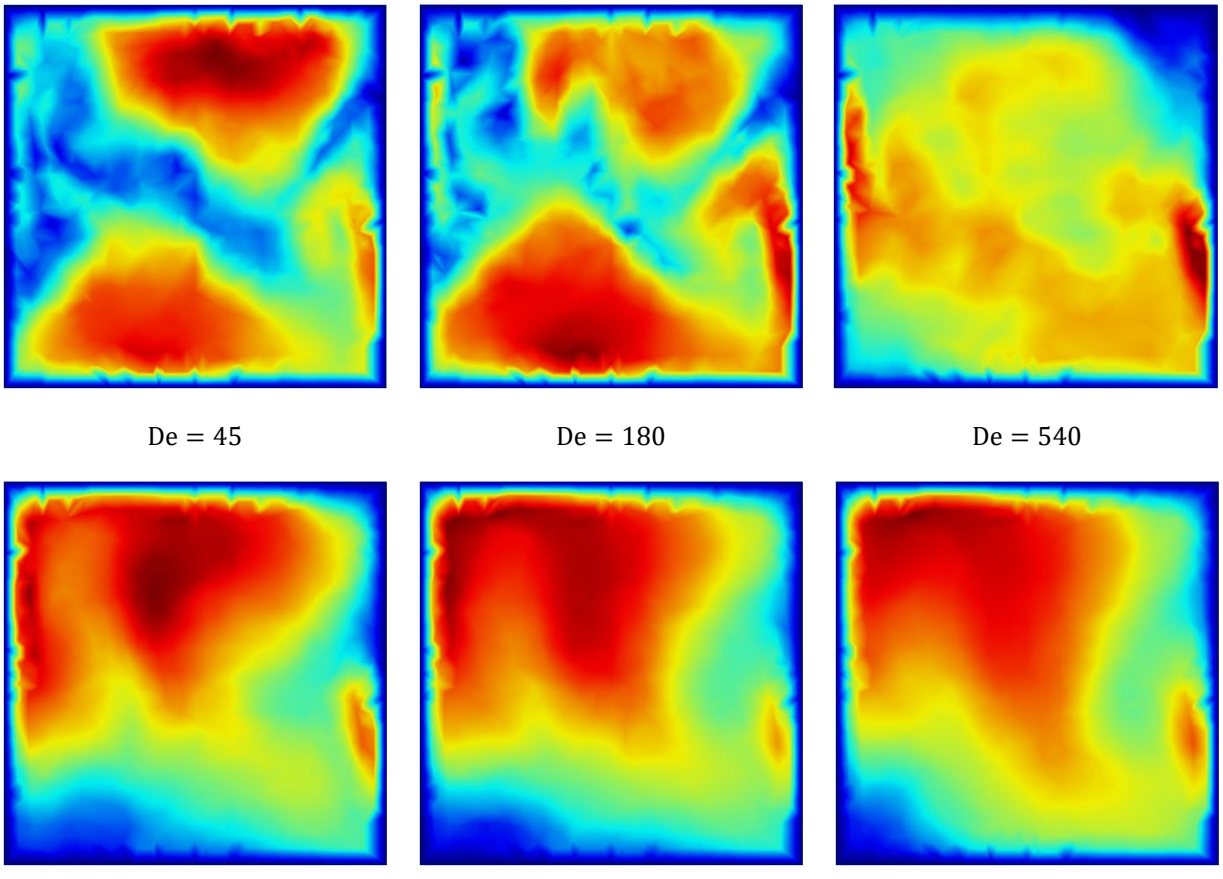

De = 45 De = 180 De = 540

De = 900 De = 1440 De = 1800

Fig. 7(d): Effect of Dean at Phase distribution. When L = 20m, Ha = 1, ∅ = 0.0 at time t = 300^{th}s at outer domain for aspect ratio (1:1).

The phase distribution for the influence of Dean number is depicted in Fig. 7(d). When the Dean number is $De = 45\ and\ 180$, Phase 1 (the heavier fluid/engine oil) is seen to be in dynamic equilibrium in the top and bottom wall, whereas Phase 2 (the lighter fluid/water) is seen to be spread throughout the whole duct. Phase 1 is seen to reside in dynamic equilibrium in the lower wall and Phase 2 on upper wall for Dean number $De = 540$. But When Dean number $De = 900,1440\ and\ 1800$, Phase 1 is seen to reside in dynamic equilibrium in middle of the duct and Phase 2 on near the wall .

In Fig. 8, the axial flow velocity, velocity contour, and vector plot of the flow field on the cut plane are compared for different fluids at the same velocity inlet on two domains. In the outer domain, water is used, whereas the inner domain uses six distinct fluids: motor oil, kerosene, ethylene glycol, heptane, ethanol, and gasoline. Kerosene has a very low viscosity, but ethanol has a very high viscosity whenever two-phase flow is examined with different fluids (table-1).

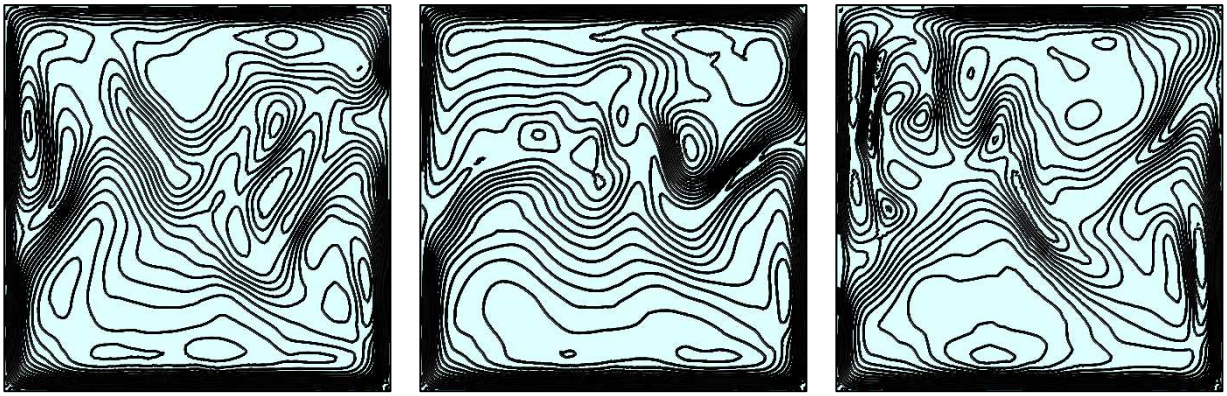

Water − Kerosene Water − Heptane Water − Engine oil

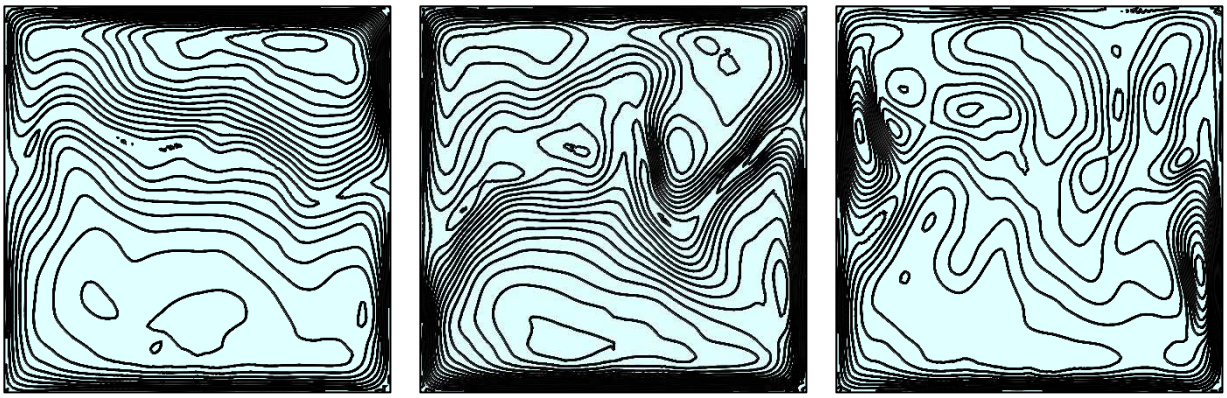

Water − Ethylene glycol Water − Gasoline Water − Ethanol

Fig. 8(a): Comparison among different fluid for velocity contour. When $\mathrm{De} = 180, \mathrm{Ha} = 1,$ $\mathrm{L} = 20\mathrm{m}$ at $\mathrm{t} = 300^{th}\mathrm{s}$ and $\emptyset = 0.0,$ at outer domain. For aspect ratio (1:1).

The mixed fluid flow for water-heptane, water-kerosene, water-gasoline, and water-ethanol generates eight to ten contours, and the axial flow is shifted near to the inner and outer walls of the duct, as displayed in Fig. 8(a). This is the reason Dean's flow is a chaos. Once more, the generation of ten to twelve via water-ethanol shows that the axial flow is shifted near to the duct's outer and inner walls. That's why Dean's flow is also chaotic. The axial flow is shifted near the top and bottom of the duct, as shown by water-ethylene glycol, which only produces two contours. Dean's flow has reached its steady state at this stage.

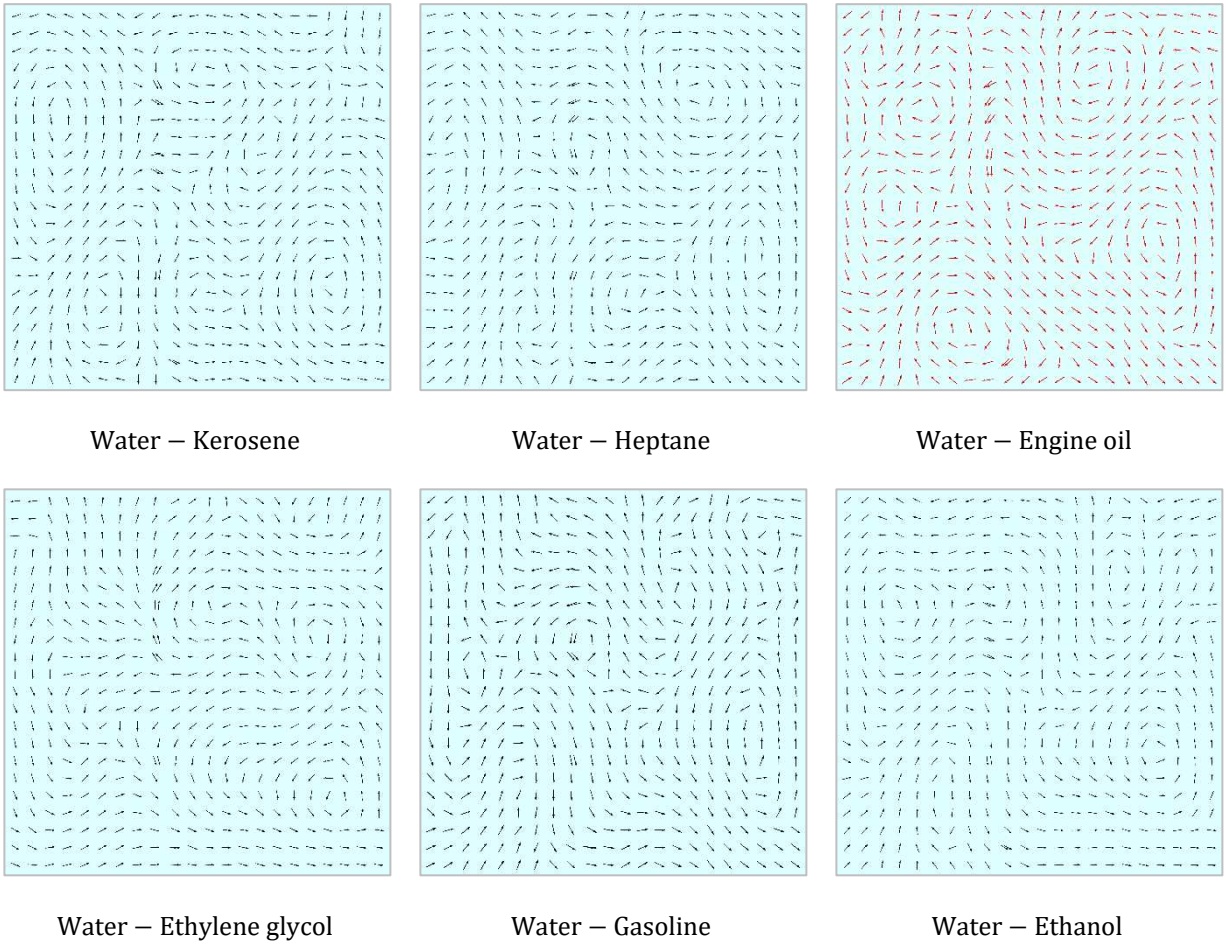

Fig. 8(b): Comparison among different fluid for vector plot of flow field. When $De = 180, Ha = 1,$ $L = 20m$ at $t = 300^{th}s$ and $\emptyset = 0.0,$ at outer domain. For aspect ratio (1:1).

Water-heptane, water-kerosene, water-gasoline, water-ethylene glycol, and water-engine oil combined fluids everyone has six symmetric vortexes solutions, and each pair of such solutions is orientated in the opposite direction (see Fig. 8(b)). Two symmetric and two asymmetric vortex

formations can be found in reverse for water-ethanol. It also shows that the direction of symmetric vortexes is opposite.

According to Fig. 8(c), the mixed fluid flow velocity for water-heptane, water-kerosene, water-ethylene glycol, water-gasoline, and water-engine oil has a hyperbolic form with numerous orbits. However, water-ethanol mixtures have a curved axial flow velocity. Additionally, it shows that for water-heptane, water-kerosene, water-gasoline, water-ethanol, and water-engine oil, the velocity of high viscosity fluids is higher than that of low viscosity fluids. Reversely, the combined flow of water and ethylene-glycol is likewise hyperbolic in shape with only two orbits, and the velocity of the low-viscosity fluid is higher than that of the high-viscosity fluid.

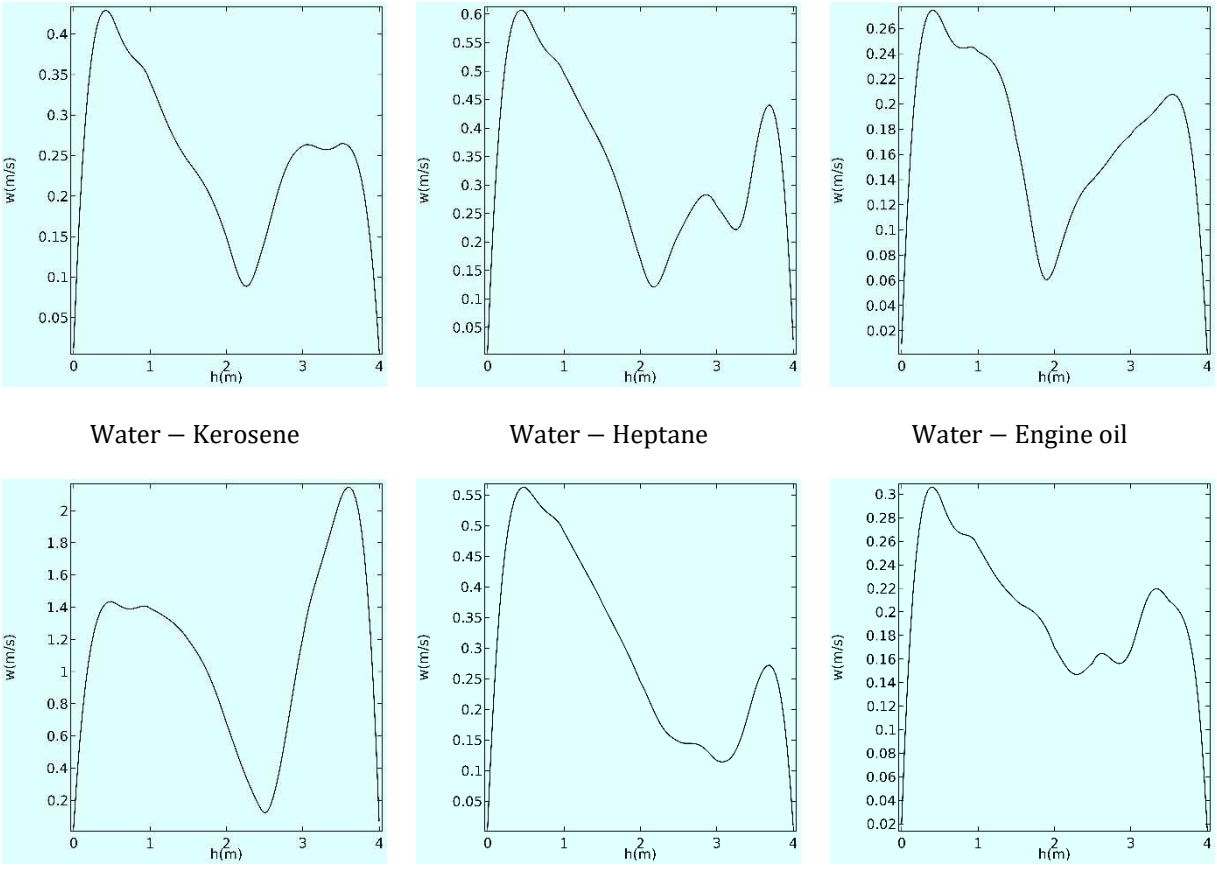

Fig. 8(c): Comparison among different fluids for axial flow velocity. When $\mathrm{De} = 180, \mathrm{Ha} = 1,$ $\mathrm{L} = 20\mathrm{m}$ at $\mathrm{t} = 300^{th}\mathrm{s}$ and $\emptyset = 0.0,$ at outer domain. For aspect ratio (1:1).

A comparison of several fluid phase distributions is shown in fig. 8(d). When water-engine oil, water-heptane, water-kerosene, or water-gasoline is present, phase 1 appears to be in dynamic

equilibrium in the upper and lower walls, and phase 2 is dispersed throughout the duct. However, Phase 1 of the water-ethylene glycol mixture be observed to be in dynamic equilibrium at the upper and lower walls, while Phase 2 is seen to be in the center. When of the water-ethanol phase 1 is observed to be in dynamic equilibrium on the lower wall and phase 2 to be in dynamic equilibrium on the top wall.

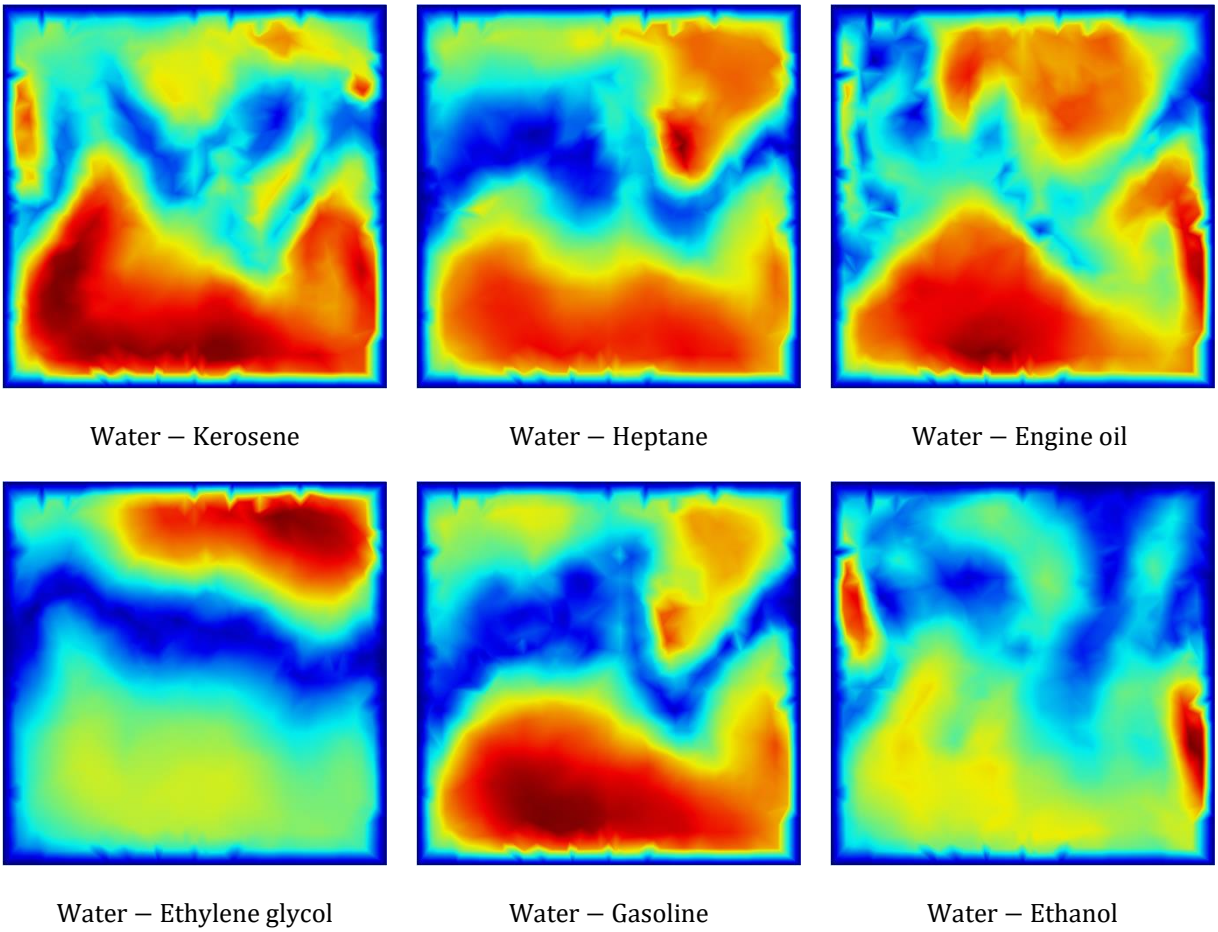

Fig. 8(d): Comparison among different fluids for phase distribution. When $De = 180, Ha = 1,$ $L = 20m$ at $t = 300^{th}s$ and $\emptyset = 0.0,$ at outer domain. For aspect ratio (1:1).

The influence of aspect ratio on the velocity contour is shown in Fig. 9(a). Axial flow is shifted closer to the duct's outer wall when the aspect ratio is (1:1), generating twelve contours. It demonstrates that there are four to six contours and that the axial flow is shifted close to the centre of the duct channel for aspect ratios of (1:2), (1:3), and (1:4). Therefore, Dean's flow is chaotic. However, when the aspect ratio is (1:5) or (1:6), it is visible that there are only two contours and that the axial flow is shifted near to the inner wall and the center of the duct channel. In this respects, Dean's flow is becoming steady. The centrifugal force forces the liquid to flow radially

from the inner to the outer duct wall because it has enough space to use it, generating lateral fluid circulation.

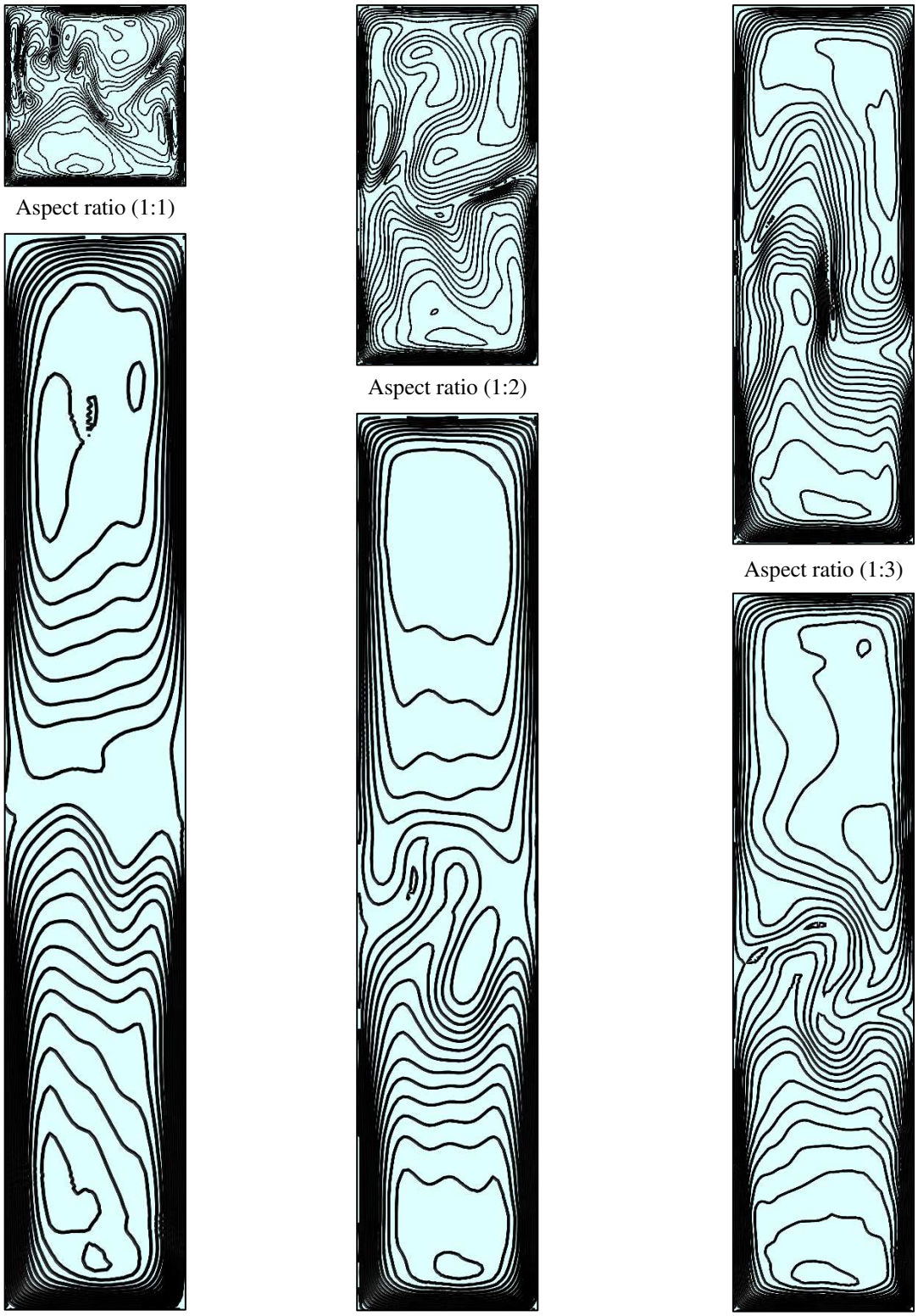

Aspect ratio (1:1)

Aspect ratio (1:2)

Aspect ratio (1:3)

Aspect ratio (1:6)

Aspect ratio (1:5)

Aspect ratio (1:4)

Fig. 9(a): Aspect ratio effect on velocity contour. When $L = 20m$, $De = 180$, Ha=1 at $t = 300^{th}s$ and $\emptyset = 0.0$ at outer domain.

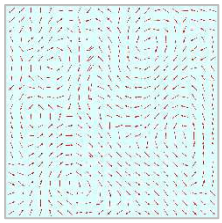

Aspect ratio (1:1)

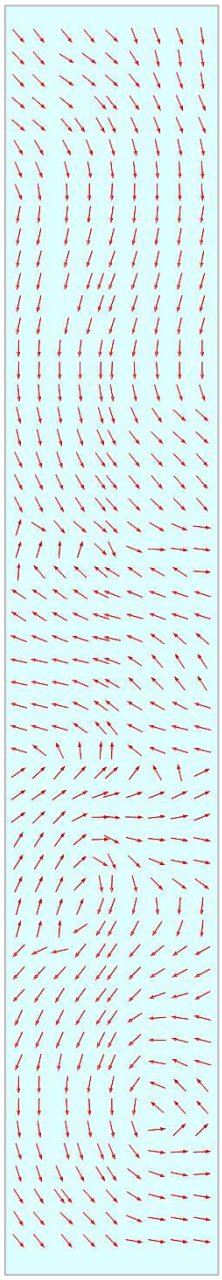

Aspect ratio (1:6)

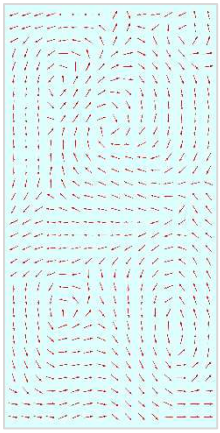

Aspect ratio (1:2)

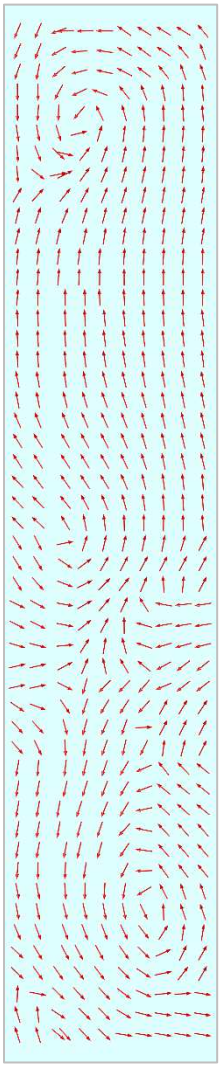

Aspect ratio (1:5)

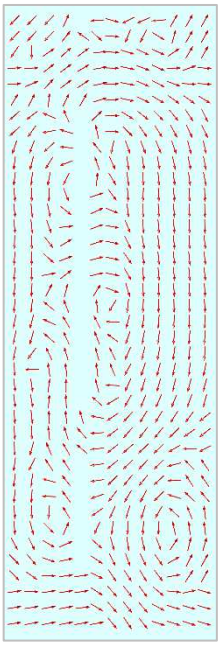

Aspect ratio (1:3)

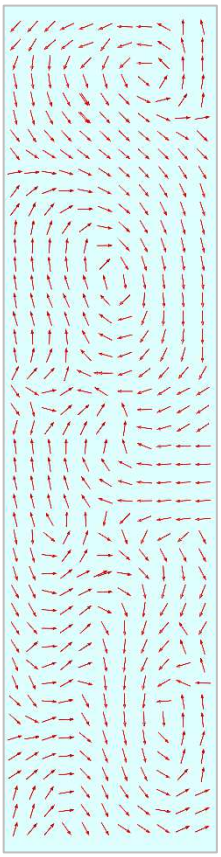

Aspect ratio (1:4)

Fig. 9(b): Aspect ratio effect on vector plot of flow field. When $L = 20m$, $De = 180$, Ha=1 at $t = 300^{th}s$ and $\emptyset = 0.0$ at outer domain.

The aspect ratio effect on the vector plot of the flow field (Dean vortex) is shown in Fig. 10(b). Secondary flow has six and four symmetric vortex solutions (the Dean vortex) when aspect ratios are (1:1) and (1:2), respectively, and each pair of vortex pairs is in the opposite direction. When

aspect ratios are (1:3) and (1:4), secondary flow has two symmetric vortices (Dean vortex) and two asymmetrical vortices. Asymmetric vortex pairs flow in a direction normal to the top wall, whereas symmetric vortex pairs flow in the opposite direction. Similarly, when aspect ratios are (1:5) and (1:6), two asymmetric secondary flow vortices are positioned on the upper and lower walls, and their trajectories are opposite.

The impact of aspect ratio on axial flow velocity is seen in Figure 10(c). The shapes are hyperbolic and have several orbits for the aspect ratios (1:1), (1:2), (1:3), (1:4), (1:5), and (1:6). High viscosity fluid seems to have a higher axial velocity than low viscosity fluid provides.

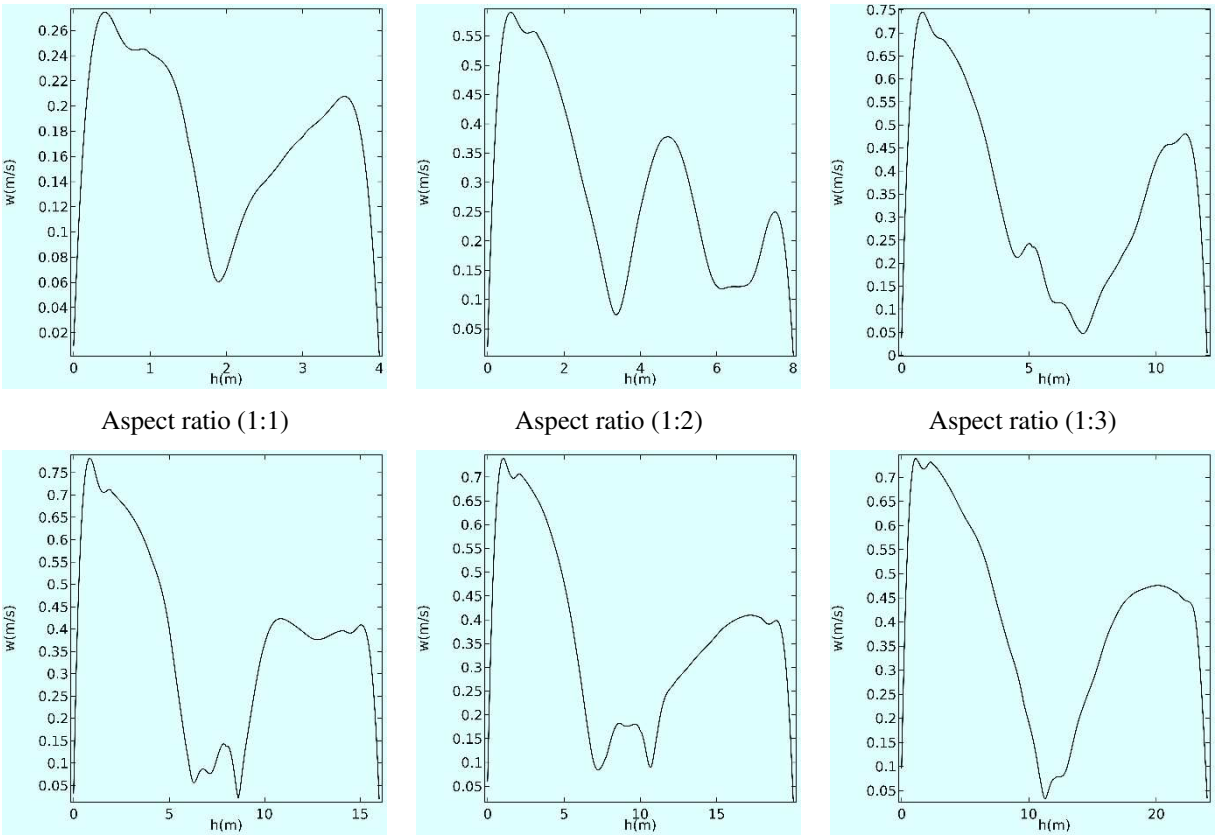

Aspect ratio (1:1) Aspect ratio (1:2) Aspect ratio (1:3)

Aspect ratio (1:4) Aspect ratio (1:5) Aspect ratio (1:6)

Fig. 9(c): Aspect ratio effect on axial flow velocity. When $L = 20m$, $De = 180$, $t = 300^{th}s$ and $\emptyset = 0.0$ at outer domain.

Fig. 10 depicts the average magnitude of the velocity of the surface on the cut plane. Fig. 10(a) depicts the effect of radius of curvature. It has been found that when the radius of curvature increases, the velocity increases. The velocity behavior is similar to a straight duct for$L \geq 100$. The Dean number's impact on the average surface velocity on the cut plane is seen in Fig. 10(b). The velocity line similarly increases as the dean number increases. Because the inlet velocity and

Reynolds number both have an impact on the Dean number. Fig.10(c) signify the effect of Hartmann number on average value of velocity magnitude. Shows that the velocity is decreasing due to increasing of Hartmann number. Fig.10(d) express that average value of velocity magnitude of surface on the cut plane increases due to decreasing of viscosity.

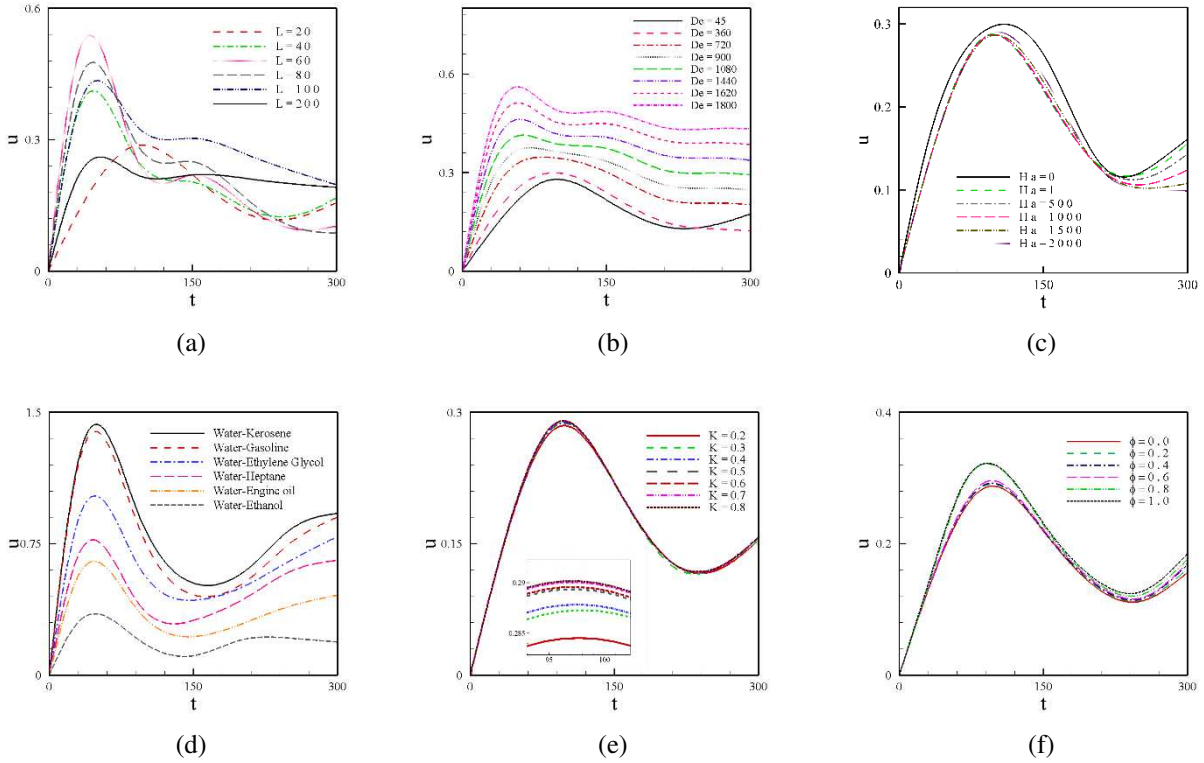

(a) (b) (c)

(d) (e) (f)

Fig. 10: Average value of velocity magnitude of surface on the cut plane (a) for effect radius of curvature, (b) for effect of Dean number, (c) for effect of Hartmann number, (d) Comparison of different fluid, (e) for effect porosity and (f) for effect of particle concentration on outer domain.

From fig.10(e), it is found velocity is increases due to increasing of porosity. The effect of particle concentration on average value of velocity magnitude of surface on the cut plane established on fig. 10(f). When particle concentration increases on outer domain the velocity is also increases.

Conclusion

The effect of magnetohydrodynamics on two-phase fluid flow in three dimensions via a porous media through a curved duct with square and rectangular cross-sections was calculated. The principal results of the investigation are summarized in the list above.

- As the radius of curvature increases, the number of contours declines and the Dean flow changes from chaotic to steady.

- As the Dean number rises, the number of vortices decreases and the Dean flow changes from chaotic to periodic.
- When the aspect ratio is changed from (1:1) to (1:6), there are fewer vortices and the flow changes from periodic to sustained.
- It is clear by observing the two-phase flows of various fluids that the flow is more steady for the fluid with low viscosity than for the fluid with high viscosity.
- When the radius of curvature is small, the velocity line is high; as the radius of curvature increases, the velocity line is low. The velocity behavior approaches that of a straight channel for large curve radius.
- The velocity line is gradually increasing as a result of an increased dean number.
- The velocity decreases with an increase in the Hartmann number. The Dean vortex increases with an increase in the Hartmann number.
- The average surface velocity magnitude on the cut plane increases as viscosity increases.

Acknowledgment

This work is done within the framework of the Ph.D. program of the first author under the Department of Mathematics, Bangladesh University of Engineering and Technology (BUET), Dhaka, Bangladesh.

Funding

Financial support from the University Grant Commission (UGC), Bangladesh Fellowship program is acknowledged.

Declaration of competing interest

The authors have no competing interests to declare that are relevant to the content of this article.

Reference

[1] J. Eustice, “Flow of water in curved pipes.”, Proceedings of the Royal Society of London. Ser. A 84(1910), 107-118.

[2] J. Eustice, “Experiments on streamline motion in curved pipes.”, Proceedings of the Royal Society of London Ser. A 85(1911), 119-131.

[3] W.R Dean, “Note on the motion of fluid in a curved pipe.”, Philosophy Magazine, 20(1927), 208-223.

[4] W.R. Dean, “The stream-line motion of fluid in a curved pipe. “Philosophy Magazine,30(1928), 673-695.

[5] S. Thangam, N. Hur, “Laminar secondary flows in curved rectangular ducts.”, Journal of Fluid Mechanics 217(1990), 421-440.

[6] S.A. Khuri, “Stokes flow in curved channels.”, Journal of Computational and Applied Mathematics 187 (2006) 171–191.

[7] S. Nadeem and Iqra Shahzadi, “Mathematical analysis for peristaltic flow of a two-phase nanofluid in a curved channel.”, Communication of Theoretical Physics 64 (2015), No-5, 547–554.

[8] R. N. Mondal, M. M. Alam, S. Yanase, “Numerical prediction of non-isothermal flows through a rotating curved duct with square cross section”, Thommasat Int. J. Sci and Tech. 12(3) (2007) 24–43.

[9] M. Norouzi and N. Biglari, “An analytical solution for Dean flow in curved ducts with rectangular cross-section, AIP, Physics of Fluids”, 25(2013), 053602.

[10] Kyoji Yamamoto, Shinichiro Yanase, and Md. Mahmud Alam, “Flow through a rotating curved duct with square cross-section”, Journal of the Physical Society of Japan, April-68(1999), No.4, 1173-1184.

[11] Z. F. Dong and M. A. Ebadian, “Effects of Buoyancy on Laminar Flow in Curved Elliptic Ducts.”, Journal of Heat Transfer, November-114(1992),936-943.

[12] P. M. Ligrani and C. R. Hedlund, “Examined surface heat transfer and flow structure in a curved channel with laminar, transitional and turbulent Flows.”, Journal of Turbomachinery, July-126(2004),414-423.

[13] A.A. Avramenko, S.G. Kobzar, I.V. Shevchuk, A.V. Kuznetsov and B.I. Basok, “Laminar Forced Convection in Curved Channel with Vortex.”, Journal of Thermal Science,13(2004), No-2,143-149.

[14] A. K. Biswas, Prasanta K Sinha, A N Mullick, B. Majumdar, “Flow Investigation in a Constant Area Curved Duct.”, International Journal of Engineering Research and Applications (IJERA), November-December -2(2012), No-6,1232-1236.

[15] Md. A. Hye, M.A.H. Khan., “Dominating Singularity of the flow in a Non-aligned Straight Rotating Pipe”, International Journal of Fluid Dynamics Research,34(2007), Issue-6, 562-571.

[16] Khan M. A. H., “Singularity Behavior of Flow in a Curved Pipe., “Journal of Applied Mechanics & Engineering,11(2006), No.3, pp. 699-704.

[17] Adrian Wegmann, Philipp Rudolf von Rohr, Two phase liquid–liquid flows in pipes of small diameters, International Journal of Multiphase Flow, 32 (2006), pp. 1017–1028.

[18] H. H. Kruse and M. Schroeder, Fundamentals of lubrication in refrigerating systems and heat pumps, International Journal of Refrigerating, 8 (1985).

[19] M. Sunami, K. Takigawa, S. Suda, New Immiscible Refrigeration Lubricant for HFCs, (1994), International Refrigeration and Air Conditioning Conference. Paper 237.

[20] Nnamdi Fidelis Okechi and Saleem Asghar (2021), “Two-phase flow in a groovy curved channel.”, European Journal of Mechanics / B Fluids 88 (2021), 191–198.

[21] P. Garg, J. R. Picardo, and S. Pushpavanam, “Vertically stratified two-phase flow in a curved channel: Insights from a domain perturbation analysis.”, Physics of fluids, 26(2014), 073604.

[22] Jason R. Picardo, P. Garg, and S. Pushpavanam, “Centrifugal instability of stratified two-phase flow in a curved channel.” Physics of fluids, 27(2015), 054106.

[23] J.L. Xu, P. Cheng, T.S. Zhao, “Gas-liquid two-phase flow regimes in rectangular channels with mini/micro gaps.”, International Journal of Multiphase Flow ,25 (1999) 411-432.

[24] Dustin Crandall, Goodarz Ahmadi and Duane H. Smith, “Comparison of experimental and numerical two-phase flows in a porous micro-model.”, Journal of Computational Multiphase Flows, Vol 1(2009). No -4.

[25] A. K. Chandra. Kishor, P. K. Mishra, and M. S. Alam, “Numerical investigations of two-phase flows through enhanced micro channels.”, Chem. Biochem. Eng. 30(2016) No- 2, 149–159.

[26] M W Al-Jibory, R S Al-Turaihi and H N Al-Jibory, “An experimental and numerical study for two-phase flow (water-air) in rectangular ducts with compound tabulators.”, Materials Science and Engineering, 433(2018), 012049.

[27] Hoque, M.M. and Alam, M.M. (2015) “A Numerical Study of MHD Laminar Flow in a Rotating Curved Pipe with Circular Cross Section”. Open Journal of Fluid Dynamics, **5**, 121-127.

[28] Chen Li, Abbas Munawwar Ali, Khadair Wissam Sadiq and Sun Bo, “Analytical solution for the MHD flow of Non-Newtonian fluids two coaxial cylinders.” Symmetry 2022,953.

[29] Vaidya H., Rajashekhar C., Prasad K.V., Khan S.U., Mebarek-Oudina F., Patil A. and Nagathan P., “Channel flow of MHD bingham fluid due to peristalsis with multiple chemical reactions: an application to blood flow narrow arteries.” SN Applied Sciences (2021) 3:186.

[30] Md. S. Alam (2016), “Numerical study on stability of magnetohydrodynamics nanofluid flow through channel.”, Ph.D. Thesis, 2016

[31] Md. S. Alam and M. A. H. Khan “Entropy Generation Analysis for Variable Thermal Conductivity MHD Radiative Nanofluid Flow through Channel.”, Journal of Applied Fluid Mechanics (2016), Vol. 9, No. 3, P.P..1123-1134.

[32] Md. S. Alam , M. A. H. Khan and M. A. Alim, “Magnetohydrodynamic Stability of Jeffery-Hamel Flow using Different Nanoparticles.” Journal of Applied Fluid Mechanics, Vol. 9, No. 2, P.P. 899-908,2016.

[33] M. K. Rahman, Md. S. Alam and M. H. Khan, “Stability of magnetohydrodynamic nanofluid flow through expanding or contracting channel with permeable walls.” Science & Technology Asia, Volume 22, No 03, P.P. 134-142,2017.

[34] Jacob Bear, “Dynamics of Fluids in Porous Media”, Elsevier, (1972), New York.

[35] R. A. Greenkorn, “Steady Flow through Porous Media.”, AIChE Journal (Vol. *27,* No. 4) July 1981, 529-545.

[36] Karuna Dwivedi, R.K. Khare, Ajit Paul, “MHD Flow through Vertical Channel with Porous Medium.”, International Journal of Applied Engineering Research, 13(2018), (15), 11923-11926.

[37] M. Devakar, K. Ramesh, Sagar Chouhan, Ankush Raje “Fully developed flow of non-Newtonian fluids in a straight uniform square duct through porous medium.” Journal of the association Arab universities Basic and Applied sciences,23(2017), Issue-1.

[38] J. Gunnar I. Hellström, “Parallel Computing of Fluid Flow Through Porous Media.” Thesis paper (2007).

[39] Subhadeep Roy, Santanu Sinha, and Alex Hansen, “Flow-Area Relations in Immiscible Two-Phase Flow in Porous Media.”, Frontiers in Physics, January 2020, Volume 8, Article 4.

[40] Raju Chowdhury, Salma Parvin, and Md. Abdul Hakim Khan, “Natural convective heat and mass transfer in a porous triangular enclosure filled with nanofluid in presence of heat generation.”, AIP Conference Proceedings, 1754, 050004; 2016.

[41] Haydar Kucuk, “Numerical analysis of entropy generation in concentric curved annular ducts.”, Journal of Mechanical Science and Technology, 24 (9) (2010), 1927-1937.

[42] T.W. Gyves, T.F. Irvine. Jr., M.H.N. Naraghi, “Gravitational and centrifugal buoyancy effects in curved square channels with conjugated boundary conditions.” International Journal of Heat and Mass Transfer 42(1999), 2015-2029.

[43] T.W. Gyves, “A numerical solution to conjugated mixed convection heat transfer in the curved square channel.”, Ph.D. Thesis, the State University of New York at Stony Brook, USA, (1997).

[44] Elin Olsson, Gunilla Kreiss, Sara Zahedi, “A conservative level set method for two phase flow II.”, Journal of Computational Physics 225 (2007) 785–807.